Journal of Polymers and the Environment (2026) 34:232
https://doi.org/10.1007/s10924-026-03955-8

ORIGINAL PAPER

Sustainable Avocado Seed Starch Nanoparticles for Limonene Encapsulation: A Novel Immunomodulatory Delivery System

Guilherme L. Alves[1] · Gislane O. Ribeiro[1] · Maria Carolina B. Di Medeiros[2] · Luciano M. Lião[2] · Luísa C. Coelho[3] · Anamélia L. Bocca[3,4,5] · Maria I.G. Leles[6] · Ricardo N. Marreto[7] · Kátia F. Fernandes[1]

Received: 14 April 2026 / Accepted: 14 August 2026

Abstract

D-limonene is a bioactive monoterpene with recognized antioxidant, anti-inflammatory, and antimicrobial properties, whose therapeutic application is severely constrained by its high volatility, sensitivity to oxidation, and poor aqueous solubility. Nanoencapsulation within biopolymeric matrices represents a promising strategy to overcome these limitations. Therefore, this study aimed to develop and characterize chemically modified avocado seed (*Persea americana* Miller) starch nanoparticles, produced via a simple one-step nanoprecipitation method, for D-limonene encapsulation, evaluating their physicochemical properties, long-term stability, and immunomodulatory potential. Acetylation of the starch was confirmed by FTIR, ^{13}C NMR, and degree of substitution (DS) determination, which collectively demonstrated successful introduction of acetyl groups into the polymer backbone and the resulting increase in hydrophobicity that underlies the encapsulation capacity of the nanocarrier. Thermogravimetric analysis further characterized the physicochemical properties of the modified starch and nanoparticles. The resulting nanoparticles displayed mean diameters lower than 350 nm, predominantly homogeneous size distributions (PdI < 0.3), zeta potentials ranging from −10.46 to −13.77 mV and encapsulation efficiency higher than 80% in two formulations. Long-term stability assessment demonstrated preservation of colloidal integrity after 10 months under refrigerated storage, with retention of approximately 69% of initial encapsulation efficiency. TEM analysis revealed small, globular particles with smooth surfaces and narrow size distribution, while FT-IR spectroscopy provided surface chemistry characterization consistent with limonene confinement within the nanoparticle core. In vitro release studies demonstrated a sustained, gradual release profile, with 59.1% of the encapsulated DL released after 24 h and release kinetics best described by a first-order model, with Fickian diffusion as the dominant transport mechanism. Immunological analysis demonstrated a potent and context-dependent immunomodulatory potential of ASNP-DL1. In vitro assays showed the suppression of pro-inflammatory cytokines (TNF-α and IL-6) in macrophages and dendritic cells, concurrently maintaining anti-inflammatory IL-10 at basal levels, indicating a coordinated shift toward an anti-inflammatory phenotype. These findings underscore the potential of this sustainable nanocarrier as a versatile platform that effectively addresses the physicochemical limitations of D-limonene, positioning this sustainable, agriculturally-derived nanocarrier as a promising candidate for immunomodulatory therapies with broad pharmaceutical and biotechnological relevance.

Keywords Starch nanoparticles · D-limonene encapsulation · Immunomodulation · Sustainable nanocarriers · Agricultural waste

Introduction

The urgency to reduce environmental impact and foster sustainable development has driven global research toward innovative solutions aligned with the principles of the circular economy and the United Nations SDGs [1]. A key strategy to achieve these goals is the valorization of agro-industrial by-products, enabling the conversion of residual streams into high-value raw materials [2, 3]. Among the possibilities, non-conventional starches are promising

Extended author information available on the last page of the article

Published online: 22 August 2026

candidates. These biopolymers are characterized by diverse physicochemical profiles, including distinct amylose contents, pasting behaviors, and functional properties that confer remarkable versatility for biotechnological applications such as encapsulation and drug delivery, without competing with the food supply chain, a critical consideration in the context of global population growth [4–6].

In this scenario, the avocado seed (*Persea americana* Miller) stands out as a significant and yet underutilized resource. Global production of avocado reaches approximately 7.5 million tons per year, and the associated by-products account for nearly 30% of the fruit's total weight, generating an estimated 2.42 million tons of waste annually worldwide. The seed (approximately 50% of the residue) is a rich source of valuable compounds, such as polyphenols and non-conventional starch [7, 8]. The high amylose content of avocado seed starch, ranging from approximately 15% to over 40% depending on botanical variety and analytical method, also confers distinct functional properties relevant to nanoparticle development, including greater resistance to retrogradation and enhanced capacity to form compact, stable matrices upon chemical modification [9].

Therefore, the strategic utilization of the avocado starch as a polymeric matrix for developing advanced drug delivery systems offers a sustainable and economically viable pathway to meet the growing global demand for natural biopolymers [7, 10, 11]. Nanoencapsulation within starch matrices has proven effective in enhancing the stability of volatile and thermolabile substances, while simultaneously improving their bioavailability and targeted delivery [12, 13].

One such bioactive compound that significantly benefits from nanoencapsulation is limonene, a major monoterpene found in *Citrus sinensis* essential oils [14, 15]. D-limonene (DL) is widely recognized for its diverse therapeutic activities, including potent antioxidant, anti-inflammatory, and antimicrobial properties [16, 17]. However, its industrial application is severely constrained by unfavorable physicochemical characteristics, such as high volatility, sensitivity to light and heat (thermo- and photolability), and poor aqueous solubility [18, 19]. Within nanoparticle systems, the hydrophobic character of DL (logP = 4.5) plays a direct mechanistic role: its affinity for the hydrophobic domains of polymeric matrices drives partitioning into the nanoparticle core during nanoprecipitation, while the surface-associated phytochemicals act as stabilizing agents that limit aggregation and modulate interfacial interactions [20]. These properties, combined with the persistent challenges of poor aqueous solubility, high volatility, and extensive phase-II metabolism that limit the oral bioavailability of citrus-derived bioactives [21], underscore the rationale for developing optimized nanocarrier systems capable of protecting and delivering DL with improved stability and controlled release [22, 23].

Despite the clear advantages of using a sustainable, non-conventional starch source for encapsulation, literature lacks studies combining avocado seed starch with the production of nanoparticles for limonene delivery. This gap represents a critical opportunity to develop an innovative delivery system that integrates circular economy principles with the optimization of a pharmacologically relevant bioactive. Furthermore, limonene itself is often extracted from orange peel residue, a by-product of the citrus industry, which further reinforces the sustainability and circularity of the proposed system [24]. Therefore, the objective of this work was to develop and fully characterize chemically modified avocado seed starch nanoparticles for the encapsulation of limonene, evaluating the efficiency of the process, the physicochemical properties of the resulting delivery system, and its immunomodulatory potential.

Materials and Methods

Materials

D-limonene (DL, 95% purity) from *Citrus sinensis* was gently provided by Agroterenas Industrial Citrus Ltda, Santa Cruz do Rio Pardo, SP, Brazil. Citric acid was acquired from Merck (Merck, Darmstadt, GER). Acetone (P.A., ACS), pyridine, N,N dimethylformamide (P.A.), and acetic anhydride were purchased from Neon Comercial Reagentes Analíticos Ltda (Suzano, SP, Brazil). All other reagents were of analytical grade. Solutions were prepared with deionized water.

Plant Material

The ripe fruits of *Persea americana* were collected from trees geographically distributed in the city of Goiânia – GO, Brazil (16°40′00″ S, 49°15′00″ W, reference point). After harvest, the fruits were packed in plastic bags and promptly delivered to the Polymer Chemistry Laboratory of the Federal University of Goiás for immediate starch extraction from the seeds.

Starch Extraction and Chemical Modification

Starch was isolated from avocado seeds according to the method described by [25], with modifications. Initially, the avocado seeds were immersed in a 1% (m/v) citric acid solution and cut into small pieces. Then, the seeds were transferred to an aqueous solution of 0.16% sodium metabisulfite and crushed, a step employed to prevent enzymatic oxidation and browning during processing, thereby preserving

starch purity and ensuring downstream nanoparticle formation is not compromised by oxidative degradation products [21]. The resulting material was filtered through a sieve (80 mesh), and the filtrate was left in an ice bath at 4 °C for 12 h. The precipitated starch was resuspended in water, and the suspension was washed by centrifugation at 5000 rpm for 5 min at 4 °C. The obtained starch was dried at room temperature (± 25 °C), lyophilized, and acetylated as described by Pitombeira et al. (2015), using acetic anhydride as acetyl donor moieties [26].

Production of Nanoparticles

The nanoparticles were synthesized using the nanoprecipitation method described by Tan et al. (2009), with modifications [27]. Initially, acetylated starch and D-limonene (DL) were dissolved in acetone (organic phase), using a septum vial to prevent DL volatilization. Distilled water was then added dropwise to the polymer suspension through the rubber septum using a 26G needle at a flow rate of 1 mL/min, maintaining a solvent-to-antisolvent ratio of 2.5:1 (v/v) (50 mL acetone:20 mL water). The addition was performed under continuous magnetic stirring at room temperature (± 25 °C) until the suspension became translucent, indicative of nanoparticle formation. For the synthesis of unloaded ASNP nanoparticles, the organic phase was prepared without DL. The residual organic solvent was removed in a vacuum concentrator (Eppendorf™ Concentrator Plus, Hamburg, Germany). Different proportions of starch were tested to optimize the nanomaterial properties, especially the encapsulation efficiency (EE%), and the nanoparticles were named as described in Table 1.

Particle Size Distribution and Zeta Potential

The hydrodynamic diameter and size distribution of the nanoparticles were evaluated by dynamic light scattering (DLS) at 25 °C using a Zetasizer Nano ZS90 (Malvern Instruments Ltd., Worcestershire, UK), with a fixed detection angle of 90°. Samples were diluted 1:10 with purified water (refractive index 1.33), and particle size distributions were analyzed using the cumulants method to obtain the Z-average diameter and polydispersity index (PdI). Zeta potential was determined by laser Doppler electrophoresis using the same equipment. All measurements were performed in triplicate and results expressed as mean ± SD.

Table 1 Components proportions of each formulation, with and without limonene

	Starch (mg)	Acetone (mL)	Water (mL)	Limonene (µL)
ASNP1	100	50	20	-
ASNP2	150	50	20	-
ASNP3	200	50	20	-
ASNP-DL1	100	50	20	50
ASNP-DL2	150	50	20	50
ASNP-DL3	200	50	20	50

Encapsulation Efficiency (EE%)

The EE% was determined by indirect UV-Vis spectrophotometry at 214 nm (KASVI K37-UV/VIS), following Ganje et al. (2019) with modifications [28]. At this wavelength, DL presents maximum absorbance, while unloaded ASNP exhibited negligible absorbance, confirming spectral selectivity. Unloaded ASNP was used as the spectrophotometric blank, so that all absorbance readings were attributed exclusively to DL. Since EE% is derived from relative absorbance ratios, no calibration curve or absolute concentration quantification was required. EE% was calculated according to Eq. (1).

$$EE\ (\%) = \left[1 - \left(\frac{ASNP - DL}{Free\ DL}\right)\right] x\ 100 \quad (1)$$

where ASNP-DL is the blank-corrected absorbance of the limonene-loaded nanoparticles and Free DL is the absorbance of the total initial DL at equivalent concentration.

Colloidal and Encapsulation Stability

The long-term stability of selected formulations (ASNP1 and ASNP-DL1) was evaluated after 10 months of storage in aqueous suspension under refrigeration (2–8 °C). At this time point, hydrodynamic diameter, PdI, and zeta potential were re-measured by DLS under the same conditions described in Sect. 2.5. The EE% of ASNP-DL1 was re-determined by UV-Vis spectrophotometry at 214 nm following the procedure described in Sect. 2.6, using a freshly prepared unloaded ASNP1 as the blank. Results were compared to freshly prepared values (t = 0) using Student's t-test, and differences were considered statistically significant at $p \leq 0.05$.

Transmission Electron Microscopy (TEM)

ASNP1 and ASNP-DL1 were also evaluated by transmission electron microscopy (TEM). A 20 µL drop of each sample was deposited onto a carbon-coated copper grid and allowed to adsorb for 10 min. Excess sample was removed by blotting with filter paper, followed by negative staining with 2% (w/v) uranyl acetate for 1 min. Grids were air-dried at room temperature and examined using a TEM JEM-2100 (JEOL, Tokyo, Japan) equipped with an EDS detector

(Thermo Scientific), operating at 200 kV, at the Laboratório Multiusuário de Microscopia de Alta Resolução (LabMic), Federal University of Goiás, Brazil.

Fourier Transform Infrared (FTIR) spectroscopy

Native and acetylated starches, and the ASNP were characterized by Fourier Transform Infrared (FTIR) spectroscopy (Bruker Vertex 70) using an Attenuated Total Reflectance (ATR) detector over the wavenumber range of 400 to 4000 cm^{-1}, with a resolution of 4 cm^{-1} and an average of 32 scans. Samples were analyzed as dry powders without further preparation. Spectra were baseline-corrected and normalized prior to comparison. The analyses were conducted in the Multiuser Analytical Center of the Chemistry Institute (CAM/IQ) at the Federal University of Goiás, Brazil.

Nuclear Magnetic Resonance Analysis (NMR)

Solid-state ^{13}C NMR experiments were performed on a BRUKER Avance III 400 spectrometer (9.4 T), operating at 75.48 MHz for the ^{13}C nucleus. Samples were loaded into a 4 mm zirconia rotor and measured with a 4 mm double-resonance CP-MAS probe at room temperature. The analysis was carried out at a spinning speed of 5–7 kHz, with a cross-polarization contact time of 34 µs, a recycle delay of 12 s, and an accumulation of 10,240 scans at room temperature, according to Mutungi et al. (2012) with modifications [29]. The degree of substitution (DS) was estimated from the solid-state ^{13}C CP/MAS NMR spectra using the methyl-to-anomeric carbon ratio method. The relative integral of the acetyl methyl carbon signal (ca. 21 ppm, CH_3) was divided by the relative integral of the anomeric carbon signal (ca. 99 ppm, C-1) of the acetylated starch spectrum, according to Eq. (2):

$$DS = \frac{I_{CH_3}}{I_{C-1}} \tag{2}$$

where I_{CH_3} and I_{C-1} represent the relative integrals of the acetyl methyl carbon and the anomeric C-1 carbon, respectively. This approach is considered appropriate for CP/MAS experiments, as both carbons are non-quaternary and respond more homogeneously to cross-polarization [29].

Thermal Analysis

The thermal behavior of ASNP was investigated by Thermogravimetric Analysis (TGA) on a DSC-60/60A analyzer (Shimadzu, Japan) at LAMES, Federal University of Goiás (UFG), Brazil. TGA measurements were carried out in platinum crucibles under a nitrogen atmosphere (50 $mL \cdot min^{-1}$), heated from 25 to 400 °C at 10 $°C \cdot min^{-1}$.

In Vitro Release Profile

The in vitro release profile of DL from ASNP-DL1 was evaluated using vertical Franz diffusion cells. A dialysis membrane (14 kDa MWCO) was hydrated for 24 h in the receptor medium prior to assembly. The donor compartment received 2 mL of ASNP-DL1 suspension, and the receptor compartment (15 mL) was filled with 10% ethanol in water, selected from a preliminary solubility screening of four media (0.1% Tween 80 in water, 10% ethanol, 50% ethanol, and 3% acetic acid) as the medium providing adequate DL solubility without membrane dissolution [30, 31]. The system was maintained at 37 ± 0.5 °C under constant stirring. Aliquots of 0.5 mL were collected from the receptor compartment at pre-determined time-intervals, with immediate replacement of an equal volume of fresh receptor medium to maintain sink conditions. The concentration of released DL was quantified by UV-Vis spectrophotometry at 214 nm. Cumulative release (Q_t, µg) was calculated correcting for the volume removed at each sampling point according to Eq. (3):

$$Q_t = C_t \, x \, V_r + \sum (C_i \, x \, V_s) \tag{3}$$

where C_t is the concentration at time t (µg/mL), V_r is the receptor volume (15 mL), C_i is the concentration at each previous collection point, and V_s is the aliquot volume (0.5 mL). Release data were fitted to zero-order, first-order, Higuchi, and Korsmeyer-Peppas kinetic models. Model selection was based on the coefficient of determination (R^2).

Analysis of Immunomodulatory Effect

These analyses were performed at the Applied Immunology Laboratory of the Institute of Biological Sciences of the University of Brasília (UnB), Brasília - DF. All immunomodulatory assays were conducted exclusively in vitro, using bone marrow-derived macrophages (BMDMs) and bone marrow-derived dendritic cells (BMDCs) obtained from C57BL/6J male mice (8–10 weeks of age) solely as a primary cell source. The use of animals was restricted to bone marrow extraction for subsequent in vitro cell differentiation, in accordance with the 3Rs principles. All procedures involving animals were approved by the Animal Ethics Committee of the University of Brasilia (UnBDoc number 66729/2016) and conducted in accordance with the Brazilian Council for the Control of Animal Experimentation (CONCEA) guidelines.

Differentiation of Bone Marrow-Derived Macrophages (BMDM) and Bone Marrow-Derived Dendritic Cells (BMDC)

Bone marrow-derived macrophages (BMDM) and dendritic cells (BMDC) were obtained according to Marina et al. (2020) [32]. Briefly, to generate pro-inflammatory M1 macrophages and dendritic cells, 2 × 10^6 cells were cultured in Roswell Park Memorial Institute (RPMI)-1640 (Thermo Fisher Scientific) medium supplemented with 10% fetal bovine serum (FBS), gentamicin, 20 ng/mL GM-CSF (ImmunoTools – Friesoythe, Germany), and 50 µM β-mercaptoethanol (Sigma-Aldrich – St. Louis, MO, USA). Medium was replenished on days 3 and 6. On day 8, dendritic cells were collected from the supernatant, while adherent macrophages were detached using TrypLE Express dissociation solution (Life Technologies – Carlsbad, CA, USA). Cells were resuspended in fresh RPMI-1640 with 10% FBS and counted, using a flow cytometer (FACSVerse – BD Biosciences – San Jose, CA, USA).

Interaction of the ASNPs with BMDM and BMDC

BMDMs or BMDCs (1×10^5 cells/well) were incubated at 37 °C in a humidified 5% CO_2 atmosphere. The culture medium was subsequently replaced with 90 µL of RPMI-1640 supplemented with 10% FBS and 10 µL of the respective samples. ASNP-DL1 and DL samples were evaluated at concentrations of 125, 250, and 500 µg/mL, expressed as limonene mass per volume. Preliminary screening across a broader range (31.25, 62.5, 125, 250, and 500 µg/mL) was performed, however no statistically significant differences were observed at the lower concentrations relative to the negative control. Thus, the three highest concentrations were selected for presentation to maintain clarity and focus on the biologically relevant range. Lipopolysaccharide (LPS, 500 ng/mL; Sigma-Aldrich) and phosphate-buffered saline (PBS, pH 7.0) were employed as positive and negative controls, respectively. Unloaded ASNP1 was also tested to determine whether the starch matrix could trigger inflammasome activation. After a 24 h incubation period (37 °C, 5% CO_2), the plates were centrifuged, and the supernatants were harvested for cytokine quantification.

Cytokine Quantification

The cell-free supernatants of the BMDM and BMDC cultures were harvested for measurement of interleukins (IL) IL-10, IL-6, and tumor necrosis factor (TNF)-α concentrations using ELISA (Ready-Set-Go! Kit – Thermo Fisher Scientific), according to the manufacturer's guidelines (Invitrogen).

Data Analysis

All cytokine quantification assays were performed in technical triplicate ($n = 3$ wells per concentration per cell type), and all remaining experiments were performed in triplicate. Results are expressed as mean ± SD. The cytokine data presented are representative of three independent experiments conducted on separate days, all of which yielded consistent results. One-way ANOVA followed by Tukey's post hoc test was applied to comparisons involving multiple groups, including physicochemical characterization of nanoparticle formulations and cytokine quantification data. Stability assessments, involving pairwise comparisons between freshly prepared and stored formulations (t = 0 vs. t = 10 months), were analyzed using Student's independent t-test. All analyses were performed using Statistica software (version 6.0, Statsoft Inc., Tulsa, USA). A p-value ≤ 0.05 was considered statistically significant.

Results and Discussions

Particle Size Distribution

Polymer amount is a crucial parameter to control nanoparticle size and distribution. If the content exceeds the critical concentration, the system may fail to achieve effective dispersion, resulting in agglomerates and heterogeneous populations. Furthermore, size and chemical composition substantially influence the interactions of nanomaterials with biological membranes, governing processes such as adhesion, internalization, and biodistribution, factors of critical relevance for the rational design and optimization of nanotherapeutics [33, 34]. Therefore, different amounts of starch were tested to optimize nanomaterial properties, and the results for mean particle diameter, zeta potential, polydispersity index (PdI), and encapsulation efficiency are presented in Table 2.

The average particle size of ASNP was below 300 nm, with a predominantly homogeneous size distribution (PdI < 0.3) in most formulations. Notably, variations in starch concentration did not significantly affect the particle size of unloaded ASNP. The incorporation of DL also had no measurable effect on the particle diameters of ASNP-DL 1 and 2, maintaining low PdI values statistically similar to those of the unloaded formulations. Conversely, ASNP-DL3 exhibited a subtly larger particle size, probably due to a combination of elevated starch concentration and DL content. Moreover, ASNP-DL3 exhibited a broader distribution (PdI = 0.35 ± 0.02), suggesting the coexistence of multiple particle populations and potential aggregation. Formulations with even higher starch content yielded larger

Table 2 Particle size, polydispersity index, zeta potential, and encapsulation efficiency of nanoparticles without and with limonene encapsulated (ASNP and ASNP-DL, respectively)

Sample Name	Particle Size (nm)	PdI	Zeta Potential (mV)	EE%
ASNP1	287.87 ± 12.24[a]	0.20 ± 0.04[a]	-16.50 ± 0.72[a]	-
ASNP2	259.23 ± 13.64[b]	0.27 ± 0.06[a]	-10.46 ± 1.16[b]	-
ASNP3	273.40 ± 11.99[a, b]	0.36 ± 0.10[a]	-10.93 ± 0.64[b]	-
ASNP-DL1	309.27 ± 12.21[a]	0.27 ± 0.04[a]	-13.77 ± 0.74[c]	85.6% ± 2.3%[a]
ASNP-DL2	294.70 ± 20.99[a]	0.23 ± 0.02[a]	-11.87 ± 0.67[b]	79.2% ± 5.7%[a]
ASNP-DL3	351.17 ± 28.54[c]	0.35 ± 0.02[b]	-11.57 ± 0.38[b]	54.8% ± 3.8%[b]

The different small superscript letters on the average data with standard deviation (±) in the same column are significantly different ($p < 0.05$)

particles, with elevated polydispersity indices (PdI > 0.7), and were consequently excluded from further analyses (data not shown).

The absence of a monotonic concentration–size relationship in the unloaded ASNP series (287, 259, and 273 nm for 100, 150, and 200 mg, respectively) is consistent with the known behavior of polysaccharide-based nanoprecipitation systems. Tan et al. (2009) demonstrated that particle size in starch acetate nanospheres prepared by nanoprecipitation increases with polymer concentration due to higher organic phase viscosity, which promotes larger nanodroplet formation, and identified a critical overlapping concentration (c*) above which PDI increases abruptly [27]. In the present study, all three starch concentrations tested appear to operate below or near this threshold, as evidenced by the statistically comparable mean diameters across ASNP1–3 (Table 2). However, concentration did influence size distribution homogeneity: PdI increased progressively from 0.20 ± 0.04 (ASNP1) to 0.36 ± 0.10 (ASNP3), reflecting a broadening of the particle population at higher polymer loads, consistent with the onset of interchain interactions that impair uniform nanoprecipitation [27, 35, 36].

The mean diameters obtained (259–351 nm) are consistent with those reported for analogous nanocarrier systems, including chitosan/alginate Pickering emulsions (ca. 274 nm) [37], alginate/collagen nanoparticles (ca. 300 nm) [38], and PLGA-based systems (ca. 280 nm) [39]. OSA-modified starch nanoparticles have been reported across a wider size range (62–248 nm) [12], reflecting the greater sensitivity of that system to formulation variables. The narrow size distributions obtained for most ASNP formulations (PdI ≤ 0.27) compare favorably with these systems and are indicative of a controlled nanoprecipitation process.

Zeta Potential

Zeta potential measurements revealed negative surface charges for all nanoparticle formulations (Table 2), consistent with previous findings involving various starch sources [40–42]. ASNP1 and ASNP-DL1 exhibited the most negative values (− 16.50 mV and − 13.77 mV, respectively), while ASNP 2 and 3, as well as ASNP-DL 2 and 3, displayed less negative surface charges (ranging from − 10.46 to − 11.87 mV). These subtle variations may be attributable to polymer content. Nanoparticles with lower polymeric load (ASNP1 and ASNP-DL1), although exhibiting comparable hydrodynamic diameters, possess reduced surface coverage, thereby exposing a greater proportion of negatively charged core functional groups. Indeed, the negative surface potential largely arises from the ionization of hydroxyl groups and the presence of phosphate esters naturally associated with amylopectin [33].

The values observed across all formulations fall below the ± 30 mV threshold conventionally associated with electrostatically stabilized dispersions. However, this criterion applies strictly to charge-stabilized systems and does not account for the steric stabilization provided by polymeric surface layers [43–45]. In acetylated starch nanoparticles, hydrophobic acetyl groups distributed along the polymer backbone reduce interfacial mobility and limit interparticle approach, providing a steric barrier that operates independently of surface charge magnitude. The low PDI values and absence of aggregation across formulations are more reliable indicators of practical colloidal stability than zeta potential alone and are consistent with this mechanism. Similar low-to-moderate zeta potential values have been reported for analogous systems: Apostolidis et al. (2023) found values between − 13.34 and − 21.56 mV for starch nanoparticles produced by nanoprecipitation [43], and Cerqueira et al. (2019) reported − 14.8 to − 18.1 mV for acetylated galactomannan micelles, both with maintained colloidal integrity [46].

Encapsulation Efficiency (EE%)

The EE% of the ASNP-DL1 and ASNP-DL2 systems was consistently high (85.6 ± 2.3% and 79.2 ± 5.7%, respectively; Table 2), with no significant difference between them, indicating efficient encapsulation under these conditions. These values are comparable to those reported for alginate/collagen nanoparticles encapsulating limonene (ca. 83.6%) [38] and approach the values achieved with OSA-modified starch systems (ca. 90%) [12], which benefit from the amphiphilic character conferred by the octenyl succinate groups. These high EE% values may be attributable to the chemically favorable core environment for DL (logP = 4.5)

created by the polymer backbone, driving its preferential partitioning into the forming nanoparticle during solvent diffusion. As the organic phase disperses into the aqueous antisolvent, the polymer matrix consolidates rapidly around the hydrophobic core, kinetically trapping the DL before redistribution to the aqueous phase can occur [27].

In contrast, ASNP-DL3 exhibited markedly reduced EE% (54.8% ± 3.8%), likely due to the higher polymer concentration, which may have promoted excessive intramolecular or intermolecular interactions during the initial stages of nanoprecipitation. Such uncontrolled aggregation compromises the efficiency of the self-assembly mechanism, leading to a suboptimal dispersion and a failure to effectively partition the DL into the core. This mechanistic explanation is consistent with the observed poor colloidal stability, as evidenced by the larger particle size (351.17 ± 28.54 nm) and higher PdI (0.35 ± 0.02), which are secondary indicators of a non-uniform and less efficient formulation.

Considering the physicochemical parameters collectively, ASNP1 and ASNP-DL1 emerged as the superior formulation pair. Among the unloaded nanoparticles, ASNP1 presented the narrowest size distribution (PdI = 0.20 ± 0.04) and the highest surface charge magnitude (− 16.50 ± 0.72 mV), while maintaining a mean diameter statistically comparable to the other formulations. Its DL-loaded counterpart, ASNP-DL1, achieved the highest encapsulation efficiency (85.6 ± 2.3%), with no statistically significant difference in particle size or PdI relative to ASNP-DL2. Although ASNP-DL2 also presented high EE% (79.2 ± 5.7%), ASNP-DL1 offered a more favorable combination of colloidal homogeneity, surface charge, and encapsulation performance. ASNP-DL3, despite sharing the same preparation method, was consistently inferior across all parameters evaluated. Accordingly, ASNP1 and ASNP-DL1 were selected for all subsequent characterization and biological assays, representing the most promising formulation in terms of both physicochemical quality and encapsulation efficiency.

Colloidal and Encapsulation Stability

The physicochemical stability of ASNP1 and ASNP-DL1 was assessed after 10 months of storage in aqueous suspension under refrigeration (2–8 °C), and results are presented in Table 3.

Both formulations retained their colloidal properties throughout the storage period, with no statistically significant changes in particle size or PdI ($p > 0.05$). ASNP1 maintained a mean diameter of 231.73 ± 51.25 nm with PdI of 0.26 ± 0.05, while ASNP-DL1 presented a mean diameter of 345.00 ± 18.07 nm with PdI of 0.36 ± 0.05, both consistent with the values recorded at t = 0. The preservation of size distribution across 10 months indicates that the acetylated starch matrix confers adequate colloidal integrity under refrigerated aqueous storage, likely owing to the hydrophobic character introduced by acetylation, which reduces polymer–water interfacial mobility and limits interparticle interactions [26].

Zeta potential values showed a statistically significant reduction in magnitude for both formulations ($p < 0.05$), declining from − 16.50 ± 0.72 mV to − 11.87 ± 0.84 mV for ASNP1, and from − 13.77 ± 0.74 mV to − 10.87 ± 0.36 mV for ASNP-DL1. Despite this reduction, neither formulation crossed the threshold typically associated with colloidal instability, and the absence of concomitant increases in particle size or PdI confirms that the charge reduction did not translate into aggregation. This behavior is consistent with previously reported observations for starch-based nanoparticles stored in aqueous media, where progressive surface charge attenuation over time is attributed to rearrangement of surface functional groups and partial hydration of the polymer shell without structural disruption [43, 47].

Regarding encapsulation capacity, ASNP-DL1 exhibited a statistically significant reduction in EE% after 10 months, from 85.6 ± 2.3% to 59.1 ± 4.0% ($p < 0.05$), representing retention of approximately 69% of the initial encapsulation efficiency. This partial loss is attributable to the gradual diffusion of DL from the hydrophobic core toward the aqueous phase over extended storage, a phenomenon commonly reported for volatile and lipophilic bioactives. Li & Lu (2016) reported a continuous decline in the encapsulated ratio of DL in nanoemulsions over 98 days even at 4 °C, a finding attributed to diffusion-driven leaching of the volatile monoterpene across the interfacial film. Notably, the 69% EE% retention observed here was achieved over a period approximately three times longer than that evaluated

Table 3 Physicochemical characterization and encapsulation efficiency of ASNP1 and ASNP-DL1 at t = 0 (freshly prepared) and after 10 months of storage in aqueous suspension under refrigeration (2–8 °C)

Sample	Time point	Particle Size (nm)	PdI	Zeta Potential (mV)	EE%
ASNP1	t = 0	287.87 ± 12.24	0.20 ± 0.04	-16.50 ± 0.72	-
	t = 10 months	231.73 ± 51.25	0.26 ± 0.05	-11.87 ± 0.84*	-
ASNP-DL1	t = 0	309.27 ± 12.21	0.27 ± 0.04	-13.77 ± 0.74	85.6% ± 2.3%
	t = 10 months	345.00 ± 18.07	0.36 ± 0.05	-10.87 ± 0.36*	59.1% ± 4.0%*

* Indicates significant difference from freshly prepared values ($p < 0.05$). No statistically significant differences were observed in particle size or PdI for either formulation between time points

in analogous DL nanoemulsion systems, underscoring the protective role of the solid acetylated starch matrix relative to liquid-phase emulsion carriers, in which the absence of a continuous polymeric barrier allows more rapid and sustained cargo diffusion [48].

Transmission Electron Microscopy (TEM)

TEM analysis was employed to assess the morphological properties of the starch nanoparticles, including particle shape and size distribution, as shown in Fig. 1.

TEM micrographs revealed small, smooth-surfaced globular nanoparticles with a narrow size distribution, corroborating the results of the DLS analysis. The formulations exhibited similar geometry, with ASNP-DL1 displaying an oily-dense core aspect with characteristic lipophilic appearance, contrasting with the uniform lucent core of ASNP1, thereby suggesting successful DL encapsulation within the starch-based nanocarrier system. The sizes observed by TEM were smaller than the hydrodynamic diameters determined by DLS, consistent with the expected difference between the dehydrated nanoparticle core visualized under vacuum conditions and the hydrodynamic diameter, which includes the polymer solvation shell. This behavior was previously reported for analogous acetylated polysaccharide nanoparticles produced by nanoprecipitation [15].

The homogeneous distribution and absence of surface roughness also demonstrate the versatility of avocado starch as a polymeric matrix for bioactive encapsulation, exhibiting sufficient malleability to reduce or eliminate surface defects following the nanoprecipitation process. Furthermore, the proximity of nanoparticles without evidence of coalescence indicates good formulation stability, likely due to electrostatic repulsion from surface charges [15].

Fourier Transform Infrared Spectroscopy (FT-IR)

FT-IR spectroscopy was used to investigate the changes in the molecular structure of starch after chemical modification and nanoprecipitation. Therefore, the FT-IR spectra of native and acetylated avocado starch, ASNP1 and ASNP-DL1, are presented in Fig. 2.

Spectral analysis revealed characteristic absorption bands consistent with native starch polymers, including a prominent broad band at 3327 cm^{-1} corresponding to O-H stretching vibrations hydroxyl groups and residual moisture. The

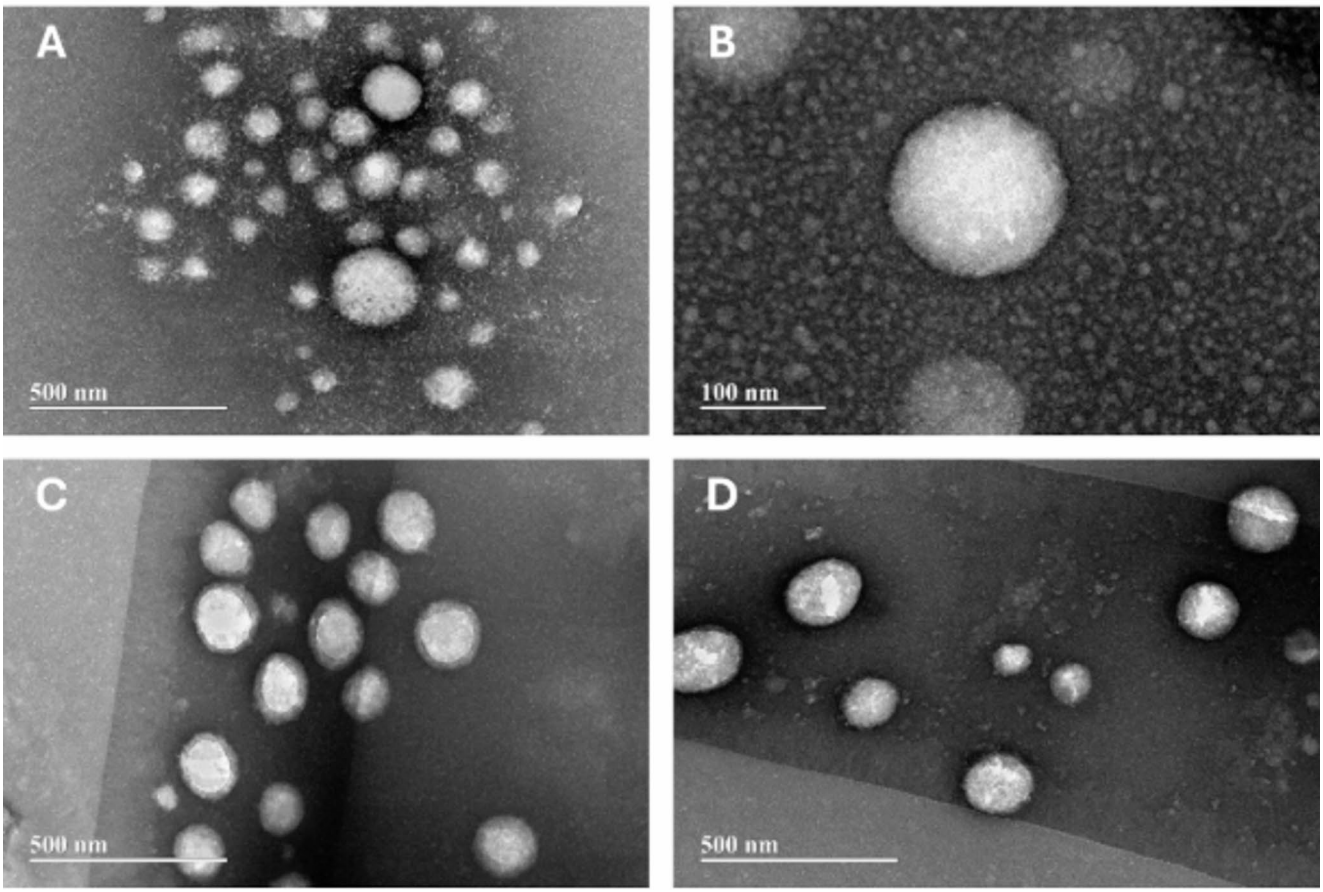

Fig. 1 TEM images of ASNP1 (A and B) and ASNP-DL1 (C and D)

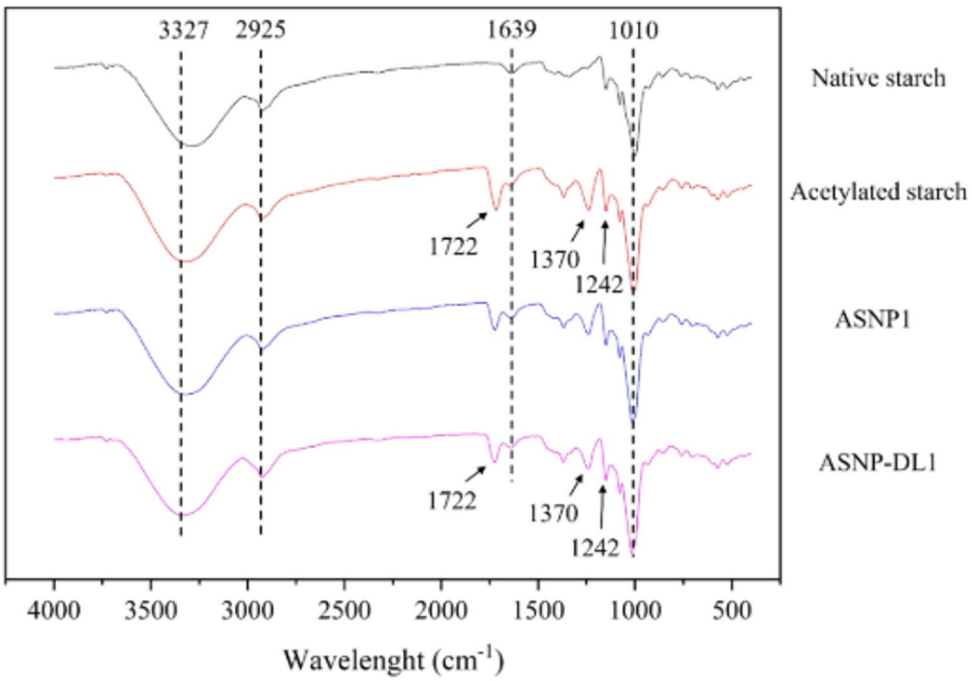

Fig. 2 FT-IR spectra of native and acetylated avocado starch, ASNP1 and ASNP-DL1

band observed at 2925 cm^{-1} was assigned to asymmetric C-H stretching vibrations of methylene (-CH_2) groups [49]. The absorption at 1639 cm^{-1} was attributed to O-H bending deformation vibrations associated with intermolecular hydrogen bonding networks characteristic of native starch architecture. Within the fingerprint region, the peak at 1242 cm^{-1} was attributed to C-O-C stretching vibrations of α-1,4 glycosidic linkages and the peak at 1010 cm^{-1} indicated C-O and C-C stretching modes within the polysaccharide framework.

Spectroscopic examination of acetylated starch revealed molecular structural modifications consequent to chemical derivatization, evidenced by the emergence of distinct absorption features. The band at 1722 cm^{-1} was assigned to C = O stretching vibrations, while the absorption at 1370 cm^{-1} corresponded to methyl group vibrational modes within the acetyl substituents [50–54].

The spectra of both ASNP1 and ASNP-DL1 preserved all characteristic absorption bands of acetylated starch, with no emergence of bands exclusively attributable to free DL. It should be noted, however, that the major vibrational modes of limonene, including C–H stretching (2966–2834 cm^{-1}), C = C stretching (1644 cm^{-1}), and CH deformation bands (1377–1243 cm^{-1}), overlap substantially with bands present in the acetylated starch matrix [55], which precludes unambiguous identification of surface-associated or free DL by FTIR alone. The primary evidence for effective encapsulation is therefore attributed to the EE% of 85.6 ± 2.3% determined by UV-Vis spectrophotometry, corroborated by the statistically larger hydrodynamic diameter of ASNP-DL1 relative to ASNP1 (309.27 vs. 287.87 nm), consistent with limonene incorporation into the nanoparticle core, and by TEM micrographs showing a dense, opaque core in ASNP-DL1 that contrasts markedly with the uniform lucent core of unloaded ASNP1.

Nuclear Magnetic Resonance Analysis (NMR)

For further information on the chemical modification, the starch samples were subjected to ^{13}C nuclear magnetic resonance (NMR), and the results are shown in Fig. 3.

Acetylation of avocado seed starch was confirmed by the appearance of signals at 172.3 ppm and 21.2 ppm, attributed to the carbonyl carbon (C = O) and methyl group (CH_3) of the acetyl moiety, respectively, which are absent in the native starch spectrum. These findings are consistent with the FTIR data, which independently confirmed the introduction of acetate ester groups through the carbonyl stretching band at 1722 cm^{-1} and the methyl deformation band at 1370 cm^{-1}. The remaining signals corresponded to the glucose backbone: a broad singlet at 72.4 ppm (C-2, C-3, and C-5), 82.8 ppm (C-4), 61.9 ppm (C-6), and a single anomeric carbon signal at 99.9 ppm (C-1), consistent with values reported by Cuenca, Ferrero, and Albani [51]. The acetylated starch spectrum displayed an amorphous character, evidenced by the broadening of the C-2, C-3, and C-5 signals relative to native starch (Fig. 3), reflecting high structural disorder attributed to the disruption of starch chain organization by the acetyl substituents, combined with the lyophilization process.

The DS, calculated as the ratio between the relative integrals of the acetyl methyl carbon (ca. 21 ppm) and the

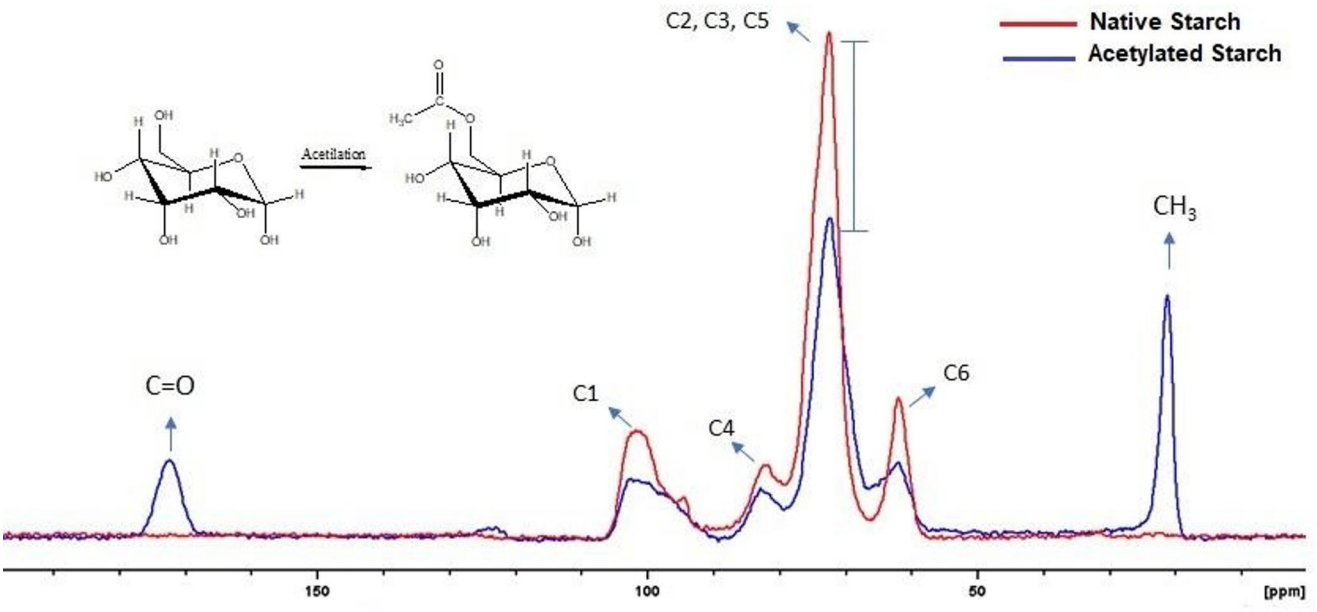

Fig. 3 Solid-state ^{13}C NMR spectra of native and acetylated avocado seed starch

anomeric carbon C-1 (ca. 99 ppm) in the solid-state ^{13}C CP/MAS NMR spectrum, yielded a value of approximately 1.15, indicating the introduction of roughly one acetyl group per glucose unit (theoretical maximum: 3). This result confirmed effective acetylation of the starch chains. Since nanoparticle formation does not involve covalent modification of the polymer backbone, the chemical identity of the acetylated starch is preserved throughout the nanoparticulation process, and the NMR characterization presented here is therefore considered representative of the polymeric matrix composing ASNP1 and ASNP-DL1. The introduction of acetyl groups, by replacing hydroxyl groups with acetyl moieties, reduces the hydrophilic character of the native starch and increases the affinity of the polymer matrix for hydrophobic molecules, a modification considered a key factor underlying the encapsulation capacity of ASNP-DL1 for DL (logP≈4.5) and the formation of a stable hydrophobic core capable of retaining the essential oil within the nanoparticle structure.

Thermal Analysis

The thermal stability of native starch, acetylated starch, ASNP1, and ASNP-DL1 was investigated by thermogravimetric analysis (TGA), and the resulting curves are presented in Fig. 4.

All samples exhibited a single major degradation event between approximately 280 and 360 °C, consistent with the thermal decomposition of the starch backbone previously reported for chemically modified starches [50, 52]. The onset of degradation did not differ substantially across samples, indicating that neither the nanoprecipitation process nor limonene encapsulation compromised the intrinsic thermal stability of the polymeric matrix.

In the low-temperature region (40–75 °C, Fig. 4 inset), native starch showed the greatest mass loss (3.43%), reflecting its high hygroscopicity. Acetylated starch (2.85%) and ASNP1 (2.96%) displayed progressively reduced mass loss, consistent with the decreased water affinity conferred by acetylation, in agreement with the FTIR and DS data discussed previously. Also, ASNP1's similar profile reflects the preservation of surface chemistry upon nanoprecipitation. Moreover, the thermogram evidenced an improved structural stability of the acetylated starch, since it has the highest residual mass in the high-temperature region (300 to 400 °C) suggesting that alterations in the molecular structure may enhanced intermolecular interactions.

Notably, ASNP-DL1 presented the lowest mass loss among all samples in this region (2.60%), falling below even that of the acetylated starch precursor. Considering DL appreciable volatility at lower temperatures, surface-adsorbed or poorly encapsulated DL would be expected to contribute additional mass loss relative to the unloaded ASNP1. Thus, the observation of a lower loss in ASNP-DL1 suggests that the monoterpene is retained within the hydrophobic nanoparticle core, where its volatilization is constrained by the polymeric matrix and where its presence may further limit water mobility at the particle interface. This interpretation is corroborated by the high encapsulation efficiency (85.6±2.3%) determined by UV-Vis spectrophotometry and by the FT-IR spectral evidence of limonene incorporation discussed in the preceding section,

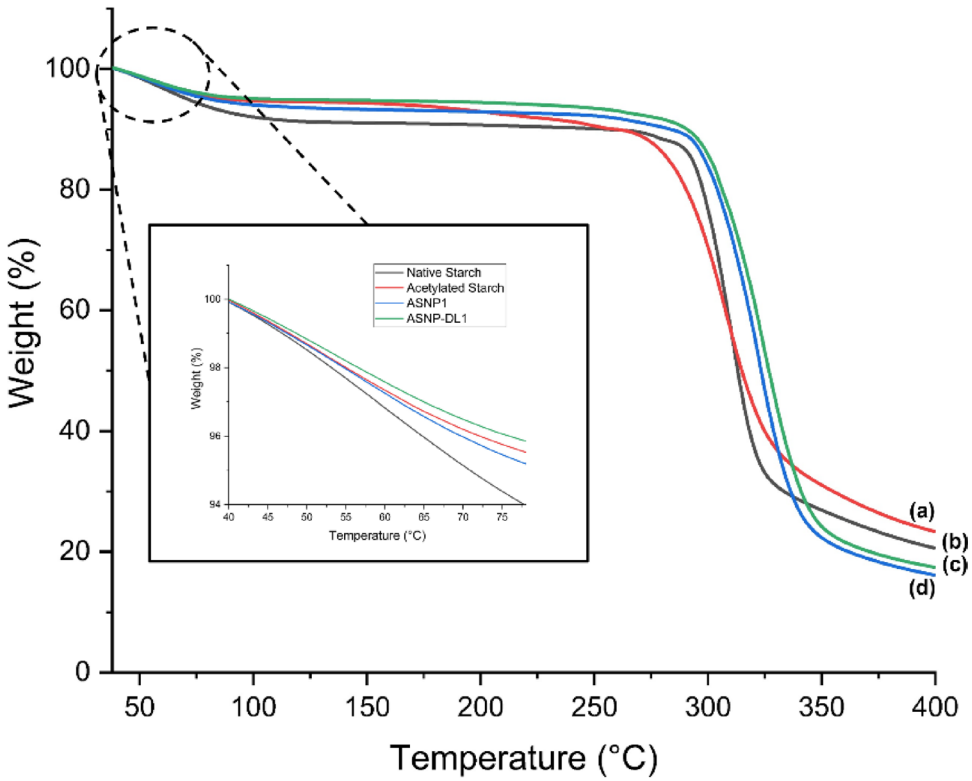

Fig. 4 TGA curves of **(a)** acetylated starch, **(b)** native starch, **(c)** ASNP-DL1, and **(d)** unloaded ASNP1. Inset: expanded view of the 40–75 °C region, highlighting differences in early mass loss associated with moisture evaporation and limonene volatility

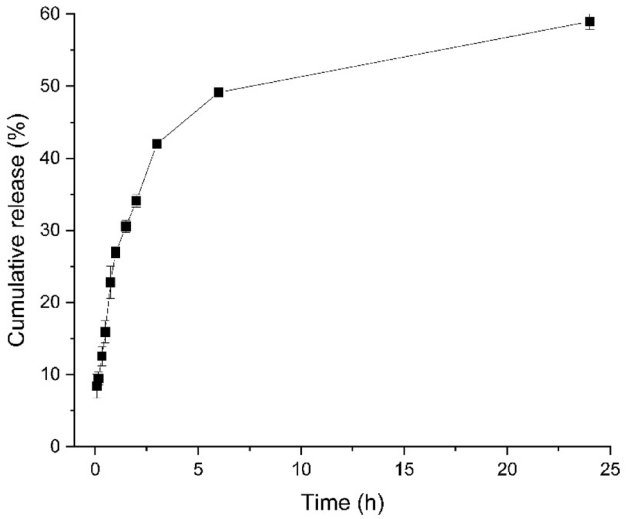

Fig. 5 In vitro cumulative release of DL from ASNP-DL1 over 24 h

collectively supporting the conclusion that limonene is effectively encapsulated rather than merely adsorbed onto the particle surface.

In Vitro Release Profile

The in vitro release profile of D-limonene from ASNP-DL1 was assessed using Franz diffusion cells over a 24 h period at 37 °C, with 10% ethanol as the receptor medium, and the resulting cumulative release curve is presented in Fig. 5.

ASNP-DL1 displayed a sustained, gradual release behavior over 24 h, reaching a total cumulative release of 59.1% (1077.4 µg) at the end of the assay (Fig. 5). An initial release of 8.4% (153.0 µg) was observed within the first 5 min, which, in the absence of detectable surface-adsorbed DL as evidenced by ATR-FTIR analysis of freshly prepared nanoparticles, is attributed to diffusion of DL located in low-density or amorphous regions of the outermost layers of the acetylated starch matrix rather than to surface adsorption. Release progressed continuously, reaching 27.0% at 60 min and 42.1% at 180 min, without evidence of a pronounced plateau during the first 3 h. A notable increase in release rate was observed between 30 and 45 min (0.459%/min), exceeding the rates in adjacent intervals (0.336%/min for 20–30 min and 0.278%/min for 45–60 min), suggesting the presence of heterogeneous populations within the matrix with distinct diffusion barriers. A relative stabilization became apparent between 6 h (49.2%) and 24 h (59.1%), where the release rate declined to 0.009%/min, indicating progressive depletion of the accessible DL fraction and the establishment of a near-plateau regime. A total of 40.9% (746.5 µg) of the initial payload remained retained in the matrix at the end of the assay, reflecting the hydrophobic interactions between DL and the acetyl groups introduced by chemical modification, which increase the affinity of the bioactive for the lipophilic domains of the polymer and restrict its diffusion into the hydroethanolic medium. This retained fraction may function as a sustained-release

reservoir whose depletion would depend on more specific in vivo solubilization conditions, a favorable attribute for controlled delivery applications.

Among the kinetic models evaluated (Table 4), the first-order model provided the best fit (R^2 = 0.950; M*max* = 53.54%; *k* = 0.0102 min^{-1}), fitted using nonlinear regression with M*max* as a free parameter according to F = M*max*·(1 − e^{−*k*t}), where F represents the cumulative release fraction (%). This model indicates that the release rate of DL is proportional to the amount of bioactive remaining within the nanoparticle matrix at each time point, a behavior consistent with concentration-driven diffusion from a finite reservoir. The finite Mmax* (53.54%) represents the theoretical asymptotic release limit estimated by the model, reflecting the existence of a fraction that would remain inaccessible under the prevailing experimental conditions. It is noteworthy that the actual cumulative release at 24 h (59.1%) slightly exceeded this modeled asymptote, a discrepancy attributable to the progressive deceleration of release observed beyond 6 h (0.009%/min between 6 and 24 h), which indicates that the system was approaching its practical release ceiling within the experimental window rather than actively releasing at rates that would substantially alter the cumulative outcome with further time. The Korsmeyer–Peppas model also yielded a satisfactory fit (R^2 = 0.939; *k* = 4.511; *n* = 0.397), and the diffusional exponent *n* < 0.45 confirms Fickian diffusion as the dominant transport mechanism, in which DL migrates through the acetylated starch matrix following a concentration gradient without significant contribution from polymer chain relaxation or swelling. The Higuchi model provided an intermediate fit (R^2 = 0.824), while the zero-order model was the least adequate (R^2 = 0.591), confirming that DL release does not follow a purely square-root-of-time dependence or a constant rate. The compact hydrophobic character of the acetylated matrix, evidenced by the increased degree of substitution (DS ≈ 1.15) and the FTIR- and NMR-confirmed presence of acetyl groups, limits water uptake and constrains polymer relaxation, mechanistically supporting the Fickian regime.

Table 4 Kinetic models fitted to the in vitro cumulative release data of D-limonene from ASNP-DL1 (Franz diffusion cells, 10% ethanol, 37 °C, 5–24 h)

Kinetic Model	Equation	R^2	Parameters	Mechanism
Zero-order	$F = F_0 + k_0 t$	0.591	k_0 = 0.0307%/min	Not applicable
First-order	$F = M_{max}(1 - e^{-kt})$	0.950	M_{max} = 53.54%; k = 0.0102 min^{-1}	Concentration-driven release from finite reservoir
Higuchi	$F = k_H \cdot t^{1/2}$	0.824	k_H = 1.490%/$min^{1/2}$	Diffusion from homogeneous matrix
Korsmeyer-Peppas	$F = kt^n$	0.939	k = 4.511; *n* = 0.397	Fickian diffusion (*n* ≤ 0.45)

F = cumulative release fraction (%); t = time (min); k = release rate constant; Mmax = maximum release (%); n = diffusional exponent. First-order model fitted using nonlinear regression with Mmax as a free parameter [F = Mmax·(1 − e^−kt)]. Highlighted row indicates best-fitting model. R^2 values calculated from 11 time points (5–24 h)

Similar diffusion-controlled profiles have been reported for limonene-loaded amylose nanostructures [28] and polysaccharide-based nanofibers [30]. Ganje et al. (2019) reported Fickian diffusion (*n* < 0.45) as the dominant mechanism for limonene release from amylose nanostructures, with first-order kinetics also providing satisfactory fits (*R* ≈ 0.94–0.98), corroborating the concentration-driven diffusion behavior observed in the present work. The cumulative release of ca. 59% at 24 h obtained for ASNP-DL1 is consistent with the controlled release range of 34–79% reported by the same authors over 6 h under intestinal conditions, reflecting the capacity of polysaccharide matrices to modulate limonene diffusion rates through hydrophobic core interactions [28].

Immunomodulatory Effect Analysis

Bone marrow-derived macrophages (BMDMs) and bone marrow-derived dendritic cells (BMDCs) are widely employed in immunological assays to quantify cytokine production due to their complementary roles in orchestrating the immune response, especially in innate responses. Macrophages primarily contribute through efficient phagocytosis and rapid cytokine secretion, thereby providing the tissue's first line of defense and shaping the local inflammatory milieu. Likewise, immature dendritic cells internalize antigens and, upon maturation, migrate from peripheral tissues to lymph nodes. Upon arrival, they become highly specialized in antigen presentation and T-lymphocyte activation, thus functioning as a critical interface between innate and adaptive immunity [56, 57]. Importantly, these two cell types differ substantially in their expression profiles of pattern recognition receptors (PRRs), including C-type lectin receptors such as Dectin-1, and Toll-like receptors, as well as in their endocytic capacity and downstream signaling repertoire, which collectively underlie their distinct functional responses to particulate stimuli [58, 59].

In this context, BMDMs and BMDCs were co-cultured and stimulated with different concentrations of DL and ASNP-DL1. TNF-α and IL-6 were selected as representative pro-inflammatory mediators rapidly induced upon innate immune cell activation, orchestrating leukocyte recruitment, vascular changes, and amplification of immune responses [42]. IL-10 was included as a counterregulatory

cytokine that limits excessive immune activation by suppressing pro-inflammatory cytokine production, antigen-presenting cell activation, and dendritic cell maturation, thereby maintaining immune homeostasis [60]. The combined analysis of these cytokines provides a mechanistically informative readout of the inflammatory phenotype adopted by immune cells in response to a given stimulus, enabling discrimination between pro-inflammatory activation, regulatory responses, and generalized immunosuppression. The results of TNF-α and IL-6 cytokine production by BMDMs are shown in Fig. 6.

Unloaded ASNP1 did not increase TNF-α secretion when administered as a single agent, demonstrating that avocado starch does not activate the BMDM inflammatory response via TNF-α-mediated mechanisms (Fig. 6A). For IL-6, the response pattern was more heterogeneous (Fig. 6B). Unloaded ASNP1 stimulated IL-6 levels of secretion (442.16 ± 5.00 pg/mL), albeit very close to negative control (PBS = 284.45 ± 23.51 pg/mL) and substantially lower than those observed with positive controls (LPS = 4,772.42 ± 137.89 pg/mL).

ASNP-DL1 and DL triggered no TNF-α production by BMDMs, with all concentrations yielding similar levels and no statistically significant differences among doses (Fig. 6A). Similarly, ASNP-DL1 maintained IL-6 secretion at near-basal levels across all tested concentrations (125 µg/mL: 306.15 ± 23.72; 250 µg/mL: 346.71 ± 16.27; 500 µg/mL: 265.65 ± 12.61 pg/mL), comparable to the negative control (PBS = 284.45 ± 23.51 pg/mL), revealing that the inflammatory effect of the unloaded ASNP1 decreased, probably due to the presence and release of the encapsulated DL. Free DL induced a marked dose-dependent reduction in IL-6 production by BMDMs, with the two highest concentrations yielding the lowest cytokine levels (77.05 ± 20.43 and 69.47 ± 15.18 pg/mL, respectively). It was an expected outcome, since the anti-inflammatory effect observed for DL is widely reported in literature [13, 19, 61, 62]. However, the distinct IL-6 modulation patterns for ASNP-DL1 and DL suggest differences in their mechanisms of action.

A different pattern was observed in dendritic cells. Data presented in Fig. 7 demonstrates that unloaded ASNP1 did not elicit inflammatory responses in BMDCs, as evidenced by the TNF-α (79.18 ± 12.24 to ASNP1 × 89.78 ± 3.78 to PBS) and IL-6 (682.01 ± 10.30 to ASNP1 × 727.50 ± 30.59 to PBS) production close to that observed with PBS.

ASNP-DL1 and DL markedly suppressed TNF-α production by BMDCs, with all tested concentrations yielding lower levels compared to the LPS group, and no statistically significant differences were observed among doses (Fig. 7A). In contrast, IL-6 secretion exhibited a complex, dose-dependent modulation characterized by a distinct biphasic pattern (Fig. 7B). ASNP-DL1 treatment at concentrations of 125 µg/mL (494.07 ± 7.67 pg/mL) and 500 µg/mL (475.64 ± 7.53 pg/mL) produced comparable cytokine levels, both lower than the intermediate concentration of 250 µg/mL (256.93 ± 41.03 pg/mL). Notably, all treatment groups remained below negative control values (PBS = 727.50 ± 30.59 pg/mL), suggesting a complex, non-linear immunomodulatory mechanism. DL displayed a clear inhibitory dose-response, with progressive reductions in IL-6 secretion from 125 to 500 µg/mL.

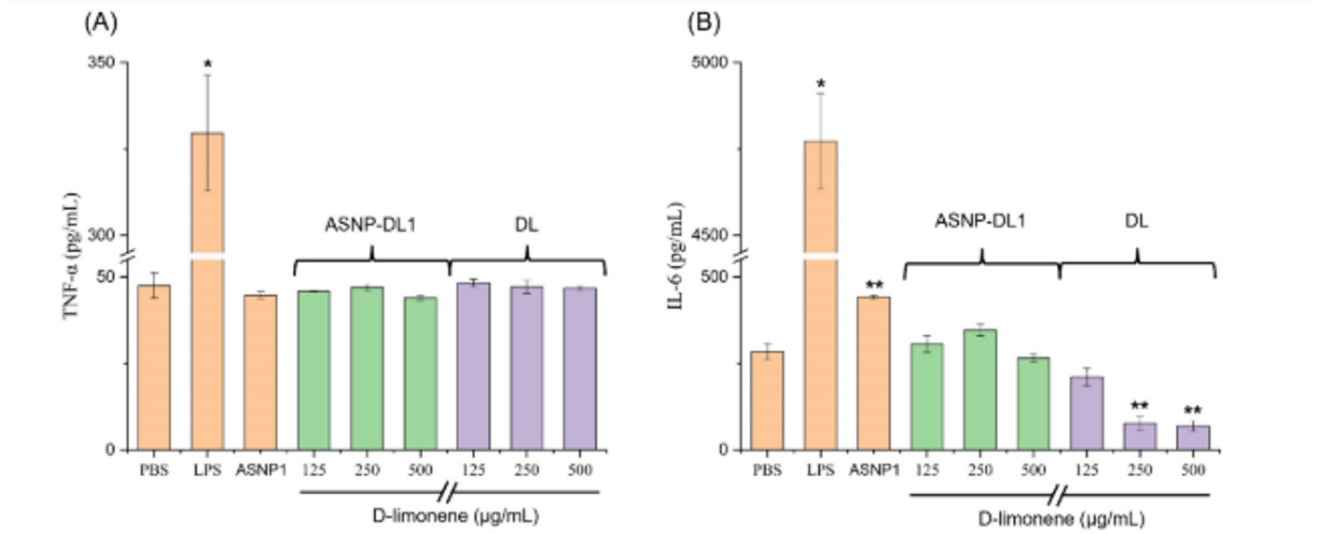

Fig. 6 Production of TNF-α (A) and IL-6 (B) by BMDMs following stimulation with ASNP-DL1 and DL at different concentrations. PBS, LPS, and ASNP1 were used as controls. * Indicates significant difference compared to the negative control (PBS); ** indicates significant difference compared to both the positive (LPS) and negative controls (PBS). All comparisons were performed using one-way ANOVA followed by Tukey's post hoc test ($p < 0.05$)

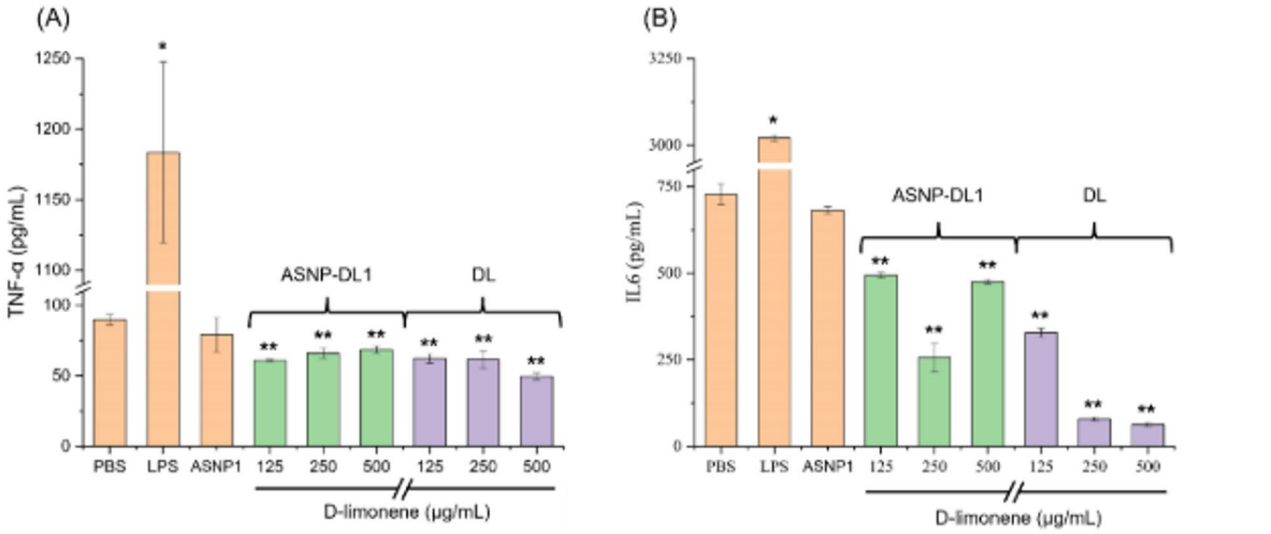

Fig. 7 Production of TNF-α (A) and IL-6 (B) by BMDCs following stimulation with ASNP-DL1 and DL at different concentrations. PBS, LPS, and ASNP1 were used as controls. * Indicates significant difference compared to the negative control (PBS), and ** indicates significant difference compared to both the positive (LPS) and negative controls (PBS). All comparisons were performed using one-way ANOVA followed by Tukey's post hoc test ($p < 0.05$)

The divergent cytokine profiles elicited by ASNP-DL1 and free DL suggest that nanoencapsulation fundamentally alters the mode of cellular exposure to the bioactive. Free DL, being immediately and fully bioavailable in the culture medium, produced a pronounced, concentration-dependent suppression of IL-6 in both BMDMs and BMDCs, consistent with direct interaction of the monoterpene with pro-inflammatory signaling pathways. ASNP-DL1, by contrast, exhibited a distinct and less linearly dose-dependent profile, which may be partly explained by the sustained release kinetics characterized for this formulation. The first-order release profile obtained indicates that only a fraction of the encapsulated DL is available at any given time point: approximately 26.9% was released within the first hour, and approximately 41% of the initial payload remained retained in the matrix at the end of the 24 h assay. Although the physicochemical conditions of the Franz cell system differ from those of the cell culture environment, this profile suggests that immune cells co-incubated with ASNP-DL1 are exposed to a progressively increasing, rather than immediately maximal, DL concentration throughout the 24 h incubation period. This kinetically distinct exposure may account for the attenuated dose-dependency and divergent suppression patterns relative to the free compound, representing a plausible contributor to the observed immunomodulatory divergence.

Furthermore, unloaded ASNP1 elicited only a marginal IL-6 signal in BMDMs and was without effect in BMDCs, while ASNP-DL1 consistently suppressed pro-inflammatory cytokine production across both cell types. This contrast indicates that the anti-inflammatory activity of ASNP-DL1 is attributable to the presence of encapsulated DL rather than to the starch matrix itself.

Beyond the kinetic dimension, the cell-type-specific responses add a further layer of functional relevance. The suppression of both TNF-α and IL-6 in BMDCs, with preservation of TNF-α production in BMDMs, suggests a selective immunomodulatory profile rather than generalized cytokine suppression. In dendritic cells, the reduction of these pro-inflammatory mediators may attenuate T-cell activation and survival during early immune priming, potentially expanding T regulatory cell populations and dampening excessive adaptive immune responses [63, 64]. In macrophages, the maintenance of TNF-α responsiveness indicates that innate immune effector functions are preserved, which is a critical distinction from broad immunosuppression. This differential modulation, attenuating dendritic cell-driven adaptive amplification while maintaining macrophage-mediated innate defense, represents an attractive profile for contexts where cytokine balance is therapeutically relevant, such as autoimmune diseases and chronic inflammatory disorders.

Figure 8. Production of IL-10 by BMDMs (A) and BMDC (B) following stimulation with ASNP-DL1 and DL at different concentrations. PBS, LPS, and ASNP1 were used as controls. * Indicates significant difference compared to the negative control (PBS), and ** indicates significant difference compared to both the positive (LPS) and negative controls (PBS). All comparisons were performed using one-way ANOVA followed by Tukey's post hoc test ($p < 0.05$).

Interestingly, treatment with ASNP-DL1 maintained IL-10 secretion by BMDMs at levels comparable to those in the PBS control, regardless of concentration, suggesting

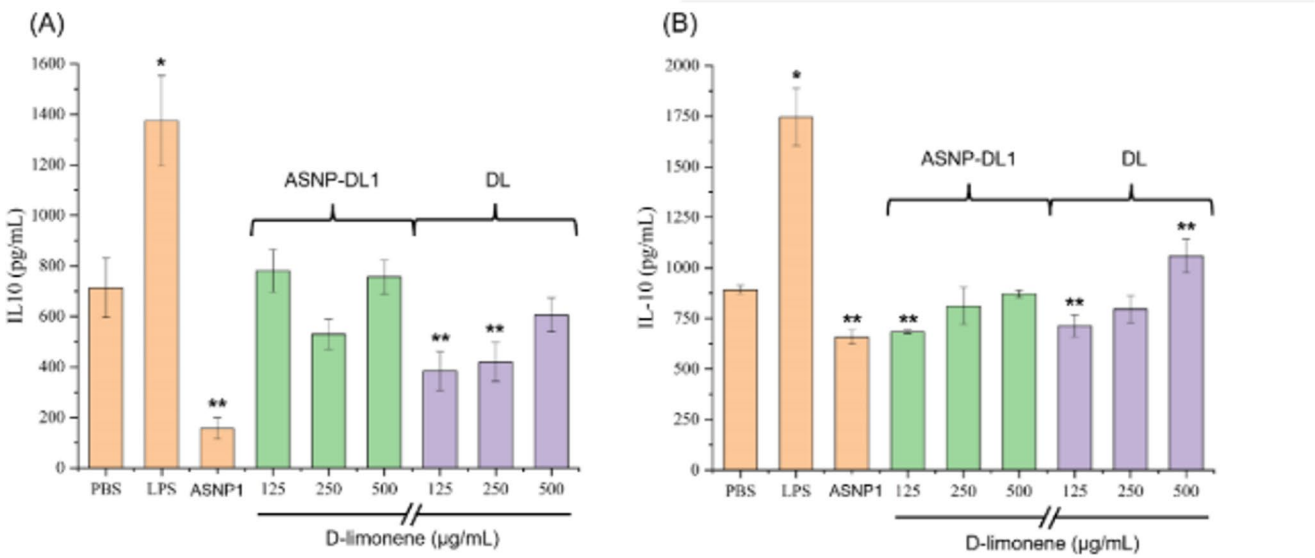

Fig. 8 shows the response profile of DL and the nanomaterials over IL-10 production by BMDMs and BMDCs. Both cells exhibited a marked increase in IL-10 secretion following LPS stimulation and the exposure to unloaded ASNP1 significantly reduced IL-10 production in both cell types

that DL-loading may counteract the suppressive effects observed with unloaded ASNP1. BMDCs exhibited reduced IL-10 production only at 125 μg/mL (683.11 ± 8.44 pg/mL), likely due to an insufficient DL load, as the levels were comparable to those observed with unloaded ASNP1 (657.22 ± 36.50 pg/mL). DL showed a dose-dependent trend, with low concentrations (125–250 μg/mL) associated with reduced or near-basal IL-10 production, whereas the highest concentration (500 μg/mL) restored or even enhanced IL-10 secretion, particularly in BMDCs.

The cytokine profiles observed across BMDMs and BMDCs reveal a cell-type-specific immunomodulatory signature for ASNP-DL1 that warrants mechanistic interpretation. The differential response of the two cell types to unloaded ASNP1, i.e. selective induction of low-level IL-6 in macrophages without a corresponding effect in dendritic cells, is consistent with known differences in PRR expression and endocytic activity between these populations. Macrophages express a broader repertoire of scavenger receptors and display higher constitutive phagocytic activity, which may favor early recognition of polysaccharide-based particulate matter and trigger low-grade innate signaling without full inflammatory activation [58, 59]. Dendritic cells, while also capable of particle internalization, rely more selectively on receptor-mediated endocytosis and are less prone to non-specific particulate uptake under resting conditions, which may explain the absence of IL-6 induction by ASNP1 in this cell type [65].

Upon DL loading, this basal starch-driven IL-6 signal in macrophages was abolished, and both cell types exhibited suppression of pro-inflammatory cytokines, with DCs additionally showing strong TNF-α inhibition. The anti-inflammatory activity of DL has been documented in several cellular and animal models, where it has been shown to inhibit pro-inflammatory mediators including TNF-α, IL-1β, and COX-2 [66, 67], and to attenuate neuroinflammation by suppressing microglial and astrocyte activation [68]. The mechanistic basis of these effects has been attributed in part to modulation of NF-κB signaling, a central transcriptional regulator of pro-inflammatory cytokine expression in innate immune cells [66]. Within the ASNP-DL1 system, the gradual release of DL, as characterized by the first-order kinetics and Fickian diffusion profile described in the release experiments, may sustain this inhibitory effect over the 24 h incubation period, potentially engaging transcriptional and post-transcriptional regulatory mechanisms that differ from those activated by the immediate, full-concentration exposure to free DL.

Notably, IL-10 was maintained at basal levels across both cell types and all ASNP-DL1 concentrations, a pattern distinct from classical immunosuppression, in which compensatory IL-10 upregulation typically accompanies the inhibition of pro-inflammatory cytokines. The maintenance of IL-10 at basal levels further suggests that the suppression of pro-inflammatory cytokines by ASNP-DL1 occurs at an early regulatory node, potentially at the level of transcriptional priming rather than downstream effector amplification, since compensatory IL-10 induction is typically observed when pro-inflammatory signals reach sufficient magnitude to trigger regulatory feedback loops [60]. This observation suggests that ASNP-DL1 promotes a coordinated shift toward an anti-inflammatory phenotype

through reduction of pro-inflammatory output, rather than through activation of the canonical IL-10-mediated regulatory axis. This profile is particularly relevant in the context of therapeutic applications where prevention of excessive inflammation is desired without compromising the regulatory capacity of the immune system, a balance that has been highlighted as critical in the management of chronic inflammatory disorders and as a desirable property of immunomodulatory nanocarriers [63–65]. Whether the molecular mechanisms underlying this selective modulation involve specific PRR engagement by the acetylated starch matrix, intracellular DL delivery following nanoparticle uptake, or a combination of both remains an open question that future mechanistic studies, including receptor-blocking assays, knockout cell models, and intracellular tracking approaches, would be well positioned to address.

When benchmarked against a broader spectrum of polymeric nanoparticles for DL delivery, ASNP-DL1 demonstrates competitive physicochemical performance and distinctive functional advantages. Critically, ASNP-DL1 achieves these metrics through a simple one-step nanoprecipitation route, without requiring the specialized processing demanded by competing systems, such as complex coacervation and autoclaving (chitosan-oleic acid) or multilayer electrostatic adsorption (soy protein isolate microcapsules) [69]. Beyond carrier performance, and in contrast to the antimicrobial [38, 70], anticancer [71], or purely physicochemical profiles reported for the comparative systems, ASNP-DL1 demonstrated context-dependent immunomodulatory activity in vitro, suppressing pro-inflammatory TNF-α and IL-6 in macrophages and dendritic cells while maintaining IL-10 at basal levels.

This dual-action functionality, combining efficient encapsulation with inherent immunomodulatory activity, has not been reported for any of the polymeric systems identified in this expanded literature survey. The sustainability advantage is particularly meaningful in the context of global food security: while conventional starch sources such as maize, cassava, and potato are increasingly disputed between food, biofuel, and materials industries, avocado seed starch is derived entirely from an agro-industrial waste stream, thereby offering a scalable, circular-economy-aligned raw material with no competition with the food supply chain. Furthermore, the amphiphilic character of acetylated starch, arising from the balance between hydrophobic acetyl groups and residual hydrophilic hydroxyl groups, suggests that this nanocarrier platform may be broadly applicable to other hydrophobic bioactives with similar physicochemical profiles, including essential oil components, lipophilic vitamins, and poorly water-soluble phytochemicals. The tunability of acetylation degree further offers a rational handle for adapting core hydrophobicity to the logP of different target compounds, expanding the translational scope of this sustainable matrix beyond the present application.

Conclusions

This study successfully developed a novel green nanomaterial using an underexploited, non-conventional starch source via a simple single-step nanoprecipitation method. Chemical modification of avocado seed starch was confirmed by FTIR, ^{13}C NMR, and degree of substitution (DS) determination, demonstrating successful acetylation and the resulting hydrophobic character that enables DL encapsulation. Thermogravimetric analysis further supported the physicochemical integrity of the modified starch and nanoparticles, with ASNP-DL1 presenting the lowest mass loss in the 40–75 °C region among all samples, consistent with effective retention of the encapsulated monoterpene within the hydrophobic nanoparticle core. Characterization by DLS, EE%, TEM, and FT-IR confirmed the suitability of avocado acetylated starch as a polymeric matrix, with ASNP-DL1 achieving encapsulation efficiencies above 80% through a one-step process. Long-term stability assessment demonstrated preservation of colloidal integrity after 10 months under refrigerated storage, with retention of approximately 69% of initial encapsulation efficiency, supporting the practical viability of the formulation. In vitro release profiling under physiological conditions demonstrated a first-order release pattern ($R^2 \approx 0.95$) with Fickian diffusion (Korsmeyer–Peppas $n \approx 0.30$), reaching approximately 59% cumulative release at 24 h. Immunomodulatory assays demonstrated that ASNP-DL1 modulates cytokine responses in a context-dependent manner. In macrophages and dendritic cells, ASNP-DL1 suppressed pro-inflammatory cytokines (TNF-α, IL-6) while maintaining anti-inflammatory IL-10 at basal levels, indicating a shift toward an anti-inflammatory phenotype. This adaptability is especially relevant for diseases where cytokine balance is critical for progression or resolution.

Collectively, these features position ASNP-DL1 as a versatile nanocarrier platform at the interface of pharmaceutical science and biotechnology, fostering the productive use of agricultural by-products and circular-economy-aligned fabrication. In vivo validation represents the logical next step to elucidate the underlying pharmacological mechanisms and advance the translational potential of this system. Further studies addressing bioavailability, pharmacokinetics, cell–nanoparticle interactions, and effective routes of administration will be essential to consolidate the considerable promise demonstrated by this formulation for immunomodulatory therapeutic applications.

Acknowledgements Acknowledgements K. F. Fernandes thanks Fundação Nacional de Desenvolvimento do Ensino Superior Particular (FUNADESP) and Conselho Nacional de Desenvolvimento Científico e Tecnológico (CNPq) for research fellowship (N° 310744/2025-3). G. L. Alves and G. O. Ribeiro thank Fundação de Amparo à Pesquisa do Estado de Goiás (FAPEG) and Coordenação de Aperfeiçoamento de Pessoal de Nível Superior (CAPES) for fellowship support. The authors thank LNF Latinoamericana for kindly supplying the enzymes used in this work.

Author contributions 1. Author ContributionsGuilherme L. Alves contributed to conceptualization, data curation, formal analysis, investigation, validation, and writing—original draft. Gislane O. Ribeiro contributed to formal analysis, investigation, and validation. Maria Carolina B. Di Medeiros contributed to conceptualization, formal analysis, investigation, and validation. Luísa C. Coelho contributed to formal analysis, investigation, and validation. Anamélia L. Bocca and Ricardo N. Marreto contributed to formal analysis and validation. Kátia F. Fernandes contributed to conceptualization, data curation, formal analysis, resources, and funding acquisition. All authors read and approved the final manuscript.

Funding The Article Processing Charge (APC) for the publication of this research was funded by the Coordenação de Aperfeiçoamento de Pessoal de Nível Superior - Brasil (CAPES) (ROR identifier: 00x0ma614). This study was supported by Fundação Nacional de Desenvolvimento do Ensino Superior Particular (FUNADESP) and the Conselho Nacional de Desenvolvimento Científico e Tecnológico (CNPq) through a research fellowship awarded to K. F. Fernandes (Grant No. 310744/2025-3). G. L. Alves has received research support from Fundação de Amparo à Pesquisa do Estado de Goiás (FAPEG).

Data Availability No datasets were generated or analysed during the current study.

Declarations

Competing interests The authors declare no competing interests.

Consent to participate Not applicable. No human participants were involved in this study.

Consent to publish Not applicable.

Ethics approval All experimental procedures involving animals were approved by the Animal Ethics Committee of the University of Brasília (UnBDoc number 66729/2016) and conducted in accordance with the guidelines of the Brazilian Council for the Control of Animal Experimentation (CONCEA). No human participants were involved in this study.

References

1. Ekmen O, Kocaman S (2024) Remote sensing for UN SDGs: A global analysis of research and collaborations. Egypt J Remote Sens Space Sci 27:329–341. https://doi.org/10.1016/j.ejrs.2024.04.002
2. Grimaldi M, Pitirollo O, Ornaghi P, Corradini C, Cavazza A (2022) Valorization of agro-industrial byproducts: Extraction and analytical characterization of valuable compounds for potential edible active packaging formulation. Food Packag Shelf Life 33:100900. https://doi.org/10.1016/j.fpsl.2022.100900
3. Maqsood S, Khalid W, Kumar P, Benmebarek IE, Rasool IFU, Trif M et al (2025) Valorization of plant-based agro-industrial waste and by-products for the production of polysaccharides: Towards a more circular economy. Appl Food Res 5:100954. https://doi.org/10.1016/j.afres.2025.100954
4. Lu Z, Lu Y, Donner E, Liu Q, Bing D (2022) Physicochemical and nutritional properties of starches from nine Canadian-grown peas compared with six commercial starches. Legume Sci 4:e133. https://doi.org/10.1002/leg3.133
5. Monu CU, Onyeka UE, Ofoedu C, Okpala COR (2025) Physicochemical characterization of sprouted cowpea starch by varieties. Qual Assur Saf Crops Foods 17:112–128. https://doi.org/10.15586/qas.v17i1.1520
6. Singh AK, Lee M, Jang D, Lee YS (2024) Non-conventional starch nanoparticles: Novel avenues towards improving sustainability of the food packaging sector. Trends Food Sci Technol 143:104273. https://doi.org/10.1016/j.tifs.2023.104273
7. Figueroa JG, Borrás-Linares I, Lozano-Sánchez J, Quirantes-Piné R, Segura-Carretero A (2025) Advanced recovery of bioactive polyphenols: integrated optimization of drying and green extraction for avocado seed by-products. Food Chem X 32:103216. https://doi.org/10.1016/j.fochx.2025.103216
8. Neves BB, Pinto S, Pais AR, Batista J, Pinho M, Goracci L et al (2025) Avocado by-products: Recycling low-cost lipids towards high-end applications. LWT 216:117376. https://doi.org/10.1016/j.lwt.2025.117376
9. Chel-Guerrero L, Barbosa-Martín E, Martínez-Antonio A, González-Mondragón E, Betancur-Ancona D (2016) Some physicochemical and rheological properties of starch isolated from avocado seeds. Int J Biol Macromol 86:302–308. https://doi.org/10.1016/j.ijbiomac.2016.01.052
10. Gutierrez-Alvarado K, Chacón-Cerdas R, Starbird-Perez R, Pectin, Microspheres (2022) Synthesis Methods, Properties, and Their Multidisciplinary Applications. Chemistry 4:121–136. https://doi.org/10.3390/chemistry4010011
11. Pires JB, Santos FN, dos, Cruz EP da, Fonseca LM, Siebeneichler TJ, Lemos GS et al (2024) Starch extraction from avocado by-product and its use for encapsulation of ginger essential oil by electrospinning. Int J Biol Macromol. ;254:127617. https://doi.org/10.1016/j.ijbiomac.2023.127617
12. Ganje M, Jamalifard R, Ghaderi S, Niakousari M (2024) Nanoencapsulation of limonene in octenyl succinic anhydride-modified starch (OSA-ST) and maltodextrin: Investigation and comparison of physicochemical properties, efficiency and morphology of nanoparticles. Heliyon 10:e39387. https://doi.org/10.1016/j.heliyon.2024.e39387
13. Huang J, Fang Z, Bai C, Mo Y, Liu D, Yang B et al (2024) Novel nano-encapsulated limonene: Utilization of drug-in-cyclodextrin-in-liposome formulation to improve the stability and enhance the antioxidant activity. Int J Pharm 653:123914. https://doi.org/10.1016/j.ijpharm.2024.123914
14. Simas DLR, Amorim SHBMD, Oliveira JMD, Alviano DS, Silva AJRD (2015) Characterization of essential oils of citrus fruits.

Citrus Res Technol [Internet]. [cited 2026 June 16];36 https://doi.org/10.5935/2236-3122.20150003
15. Silva CNS, Ferreira RDR, Campos ITN, Fernandes KF, Lião LM, Di Medeiros MCB et al (2025) Acetylated cashew gum polysaccharide nanoparticles as a promising green label nanomaterial for encapsulation of D-limonene: physicochemical, structural and antibacterial properties. Eur Food Res Technol 251:519–533. https://doi.org/10.1007/s00217-024-04649-y
16. Akhavan-Mahdavi S, Sadeghi R, Faridi Esfanjani A, Hedayati S, Shaddel R, Dima C et al (2022) Nanodelivery systems for d-limonene; techniques and applications. Food Chem 384:132479. https://doi.org/10.1016/j.foodchem.2022.132479
17. Li S, Rong L, Wang S, Liu S, Lu Z, Miao L et al (2022) Enhanced limonene production by metabolically engineered Yarrowia lipolytica from cheap carbon sources. Chem Eng Sci 249:117342. https://doi.org/10.1016/j.ces.2021.117342
18. Schutz GF, Alves RMV, Delarmelina C, Duarte MCT, Vieira RP (2024) Limonene and its derived oligomer as bioactive additives in starch/coffee husks biocomposites for food packaging applications. Int J Biol Macromol 260:129482. https://doi.org/10.1016/j.ijbiomac.2024.129482
19. Zhang L, Wang W, Wang Z, Song W, Li H, Yang J et al (2025) Biotransformation of limonene: pathways, biocatalysts, and applications. Food Biosci 69:106812. https://doi.org/10.1016/j.fbio.2025.106812
20. Khan MA, Ahmed M, Abu-Hussien SH, Zahid MU, Alharbi BF (2025) Green synthesis of iron oxide nanoparticles (Fe2O3-NPs) from Citrus Limetta agrowaste for biological and photocatalytic applications. Sci Rep 15:33107. https://doi.org/10.1038/s41598-025-17750-3
21. Zahid MU, Akhlaq H, Atta K, Javaid A, Rasheed F (2026) Fabrication, characterization, and in vivo biosafety evaluation of starch-based bioplastic as a sustainable alternative to polystyrene. Biomater Adv 181:214659. https://doi.org/10.1016/j.bioadv.2025.214659
22. Liu Z, Zhao Y, Zheng J, Wang Z, Yan X, Zhang T (2024) Physicochemical and digestive properties of corn starch nanoparticles incorporated different polyphenols. Int J Biol Macromol 265:130681. https://doi.org/10.1016/j.ijbiomac.2024.130681
23. Zahid MU, Atta K, Zahra A, Rasheed F, Kayani WK (2026) Phytochemical diversity and functional food relevance of Citrus limon and Citrus limetta. Food Biosci 76:108267. https://doi.org/10.1016/j.fbio.2026.108267
24. Siddiqui SA, Pahmeyer MJ, Assadpour E, Jafari SM (2022) Extraction and purification of d-limonene from orange peel wastes: Recent advances. Ind Crops Prod 177:114484. https://doi.org/10.1016/j.indcrop.2021.114484
25. Rupollo G, Vanier NL, Da Rosa Zavareze E, De Oliveira M, Pereira JM, Paraginski RT et al (2011) Pasting, morphological, thermal and crystallinity properties of starch isolated from beans stored under different atmospheric conditions. Carbohydr Polym 86:1403–1409. https://doi.org/10.1016/j.carbpol.2011.06.055
26. Pitombeira NAO, Veras Neto JG, Silva DA, Feitosa JPA, Paula HCB, De Paula RCM (2015) Self-assembled nanoparticles of acetylated cashew gum: Characterization and evaluation as potential drug carrier. Carbohydr Polym 117:610–615. https://doi.org/10.1016/j.carbpol.2014.09.087
27. Tan Y, Xu K, Li L, Liu C, Song C, Wang P (2009) Fabrication of Size-Controlled Starch-Based Nanospheres by Nanoprecipitation. ACS Appl Mater Interfaces 1:956–959. https://doi.org/10.1021/am900054f
28. Ganje M, Jafari SM, Tamadon AM, Niakosari M, Maghsoudlou Y (2019) Mathematical and fuzzy modeling of limonene release from amylose nanostructures and evaluation of its release kinetics. Food Hydrocoll 95:186–194. https://doi.org/10.1016/j.foodhyd.2019.04.045
29. Mutungi C, Passauer L, Onyango C, Jaros D, Rohm H (2012) Debranched cassava starch crystallinity determination by Raman spectroscopy: Correlation of features in Raman spectra with X-ray diffraction and 13 C CP/MAS NMR spectroscopy. Carbohydr Polym 87:598–606. https://doi.org/10.1016/j.carbpol.2011.08.032
30. Kamalpour R, Koocheki A, Ghorani B (2025) Encapsulation of D-limonene in Lepidium perfoliatum seed gum/PVA electrospun nanofibers: Physicochemical characterization and modeling the kinetics of release. Curr Res Food Sci 10:100966. https://doi.org/10.1016/j.crfs.2024.100966
31. Souto EB, Zielinska A, Souto SB, Durazzo A, Lucarini M, Santini A et al (2020) (+)-Limonene 1,2-Epoxide-Loaded SLNs: Evaluation of Drug Release, Antioxidant Activity, and Cytotoxicity in an HaCaT Cell Line. Int J Mol Sci 21:1449. https://doi.org/10.3390/ijms21041449
32. Marina CL, Bürgel PH, Agostinho DP, Zamith-Miranda D, Las-Casas L, de Tavares O (2020) Nutritional Conditions Modulate C. neoformans Extracellular Vesicles' Capacity to Elicit Host Immune Response. Microorganisms 8:1815. https://doi.org/10.3390/microorganisms8111815
33. Hedayati S, Niakousari M, Mohsenpour Z (2020) Production of tapioca starch nanoparticles by nanoprecipitation-sonication treatment. Int J Biol Macromol 143:136–142. https://doi.org/10.1016/j.ijbiomac.2019.12.003
34. Meena J, Goswami DG, Anish C, Panda AK (2021) Cellular uptake of polylactide particles induces size dependent cytoskeletal remodeling in antigen presenting cells. Biomater Sci 9:7962–7976. https://doi.org/10.1039/D1BM01312B
35. Bovone G, Cousin L, Steiner F, Tibbitt MW (2022) Solvent Controls Nanoparticle Size during Nanoprecipitation by Limiting Block Copolymer Assembly. Macromolecules 55:8040–8048. https://doi.org/10.1021/acs.macromol.2c00907
36. Stevanović M, Filipović N (2024) A Review of Recent Developments in Biopolymer Nano-Based Drug Delivery Systems with Antioxidative Properties: Insights into the Last Five Years. Pharmaceutics 16:670. https://doi.org/10.3390/pharmaceutics16050670
37. Li Q, Li R, Yong F, Zhao Q, Chen J, Lin X et al (2024) Modulation the Synergistic Effect of Chitosan-Sodium Alginate Nanoparticles with Ca2+: Enhancing the Stability of Pickering Emulsion on D-Limonene. Foods 13:622. https://doi.org/10.3390/foods13040622
38. Valookolaei F-SG, Sazegar H, Rouhi L (2024) Limonene encapsulated alginate/collagen as antibiofilm drug against Acinetobacter baumannii. BMC Biotechnol 24:86. https://doi.org/10.1186/s12896-024-00888-9
39. Adeyemi SB, Akere AM, Orege JI, Ejeromeghene O, Orege OB, Akolade JO (2023) Polymeric nanoparticles for enhanced delivery and improved bioactivity of essential oils. Heliyon 9:e16543. https://doi.org/10.1016/j.heliyon.2023.e16543
40. Ahmad M, Gani A, Hassan I, Huang Q, Shabbir H (2020) Production and characterization of starch nanoparticles by mild alkali hydrolysis and ultra-sonication process. Sci Rep 10:3533. https://doi.org/10.1038/s41598-020-60380-0
41. Chang R, Ji N, Li M, Qiu L, Sun C, Bian X et al (2019) Green preparation and characterization of starch nanoparticles using a vacuum cold plasma process combined with ultrasonication treatment. Ultrason Sonochem 58:104660. https://doi.org/10.1016/j.ultsonch.2019.104660
42. Remanan MK, Zhu F (2021) Encapsulation of rutin using quinoa and maize starch nanoparticles. Food Chem 353:128534. https://doi.org/10.1016/j.foodchem.2020.128534
43. Apostolidis E, Stergiou A, Kioupis D, Sadeghpour A, Paximada P, Kakali G et al (2023) Production of nanoparticles from resistant

starch via a simple three-step physical treatment. Food Hydrocoll 137:108412. https://doi.org/10.1016/j.foodhyd.2022.108412
44. Gopmandal PP, Duval JFL (2022) Electrostatics and electrophoresis of engineered nanoparticles and particulate environmental contaminants: Beyond zeta potential-based formulation. Curr Opin Colloid Interface Sci 60:101605. https://doi.org/10.1016/j.cocis.2022.101605
45. Uskoković V (2012) Dynamic Light Scattering Based Microelectrophoresis: Main Prospects and Limitations. J Dispers Sci Technol 33:1762–1786. https://doi.org/10.1080/01932691.2011.625523
46. Cerqueira MA, Pinheiro AC, Pastrana LM, Vicente AA (2019) Amphiphilic Modified Galactomannan as a Novel Potential Carrier for Hydrophobic Compounds. Front Sustain Food Syst 3:17. https://doi.org/10.3389/fsufs.2019.00017
47. Marta H, Rizki DI, Mardawati E, Djali M, Mohammad M, Cahyana Y (2023) Starch Nanoparticles: Preparation, Properties and Applications. Polymers 15:1167. https://doi.org/10.3390/polym15051167
48. Li P-H, Lu W-C (2016) Effects of storage conditions on the physical stability of d-limonene nanoemulsion. Food Hydrocoll 53:218–224. https://doi.org/10.1016/j.foodhyd.2015.01.031
49. Ferreira S, Araujo T, Souza N, Rodrigues L, Lisboa HM, Pasquali M et al (2019) Physicochemical, morphological and antioxidant properties of spray-dried mango kernel starch. J Agric Food Res 1:100012. https://doi.org/10.1016/j.jafr.2019.100012
50. Colussi R, El Halal SLM, Pinto VZ, Bartz J, Gutkoski LC, Da Rosa Zavareze E et al (2015) Acetylation of rice starch in an aqueous medium for use in food. LWT - Food Sci Technol 62:1076–1082. https://doi.org/10.1016/j.lwt.2015.01.053
51. Cuenca P, Ferrero S, Albani O (2020) Preparation and characterization of cassava starch acetate with high substitution degree. Food Hydrocoll 100:105430. https://doi.org/10.1016/j.foodhyd.2019.105430
52. Mbougueng PD, Tenin D, Scher J, Tchiégang C (2012) Influence of acetylation on physicochemical, functional and thermal properties of potato and cassava starches. J Food Eng 108:320–326. https://doi.org/10.1016/j.jfoodeng.2011.08.006
53. Olagunju AI, Omoba OS, Enujiugha VN, Wiens RA, Gough KM, Aluko RE (2020) Influence of acetylation on physicochemical and morphological characteristics of pigeon pea starch. Food Hydrocoll 100:105424. https://doi.org/10.1016/j.foodhyd.2019.105424
54. Shah A, Masoodi FA, Gani A, Ashwar BA (2017) Physicochemical, rheological and structural characterization of acetylated oat starches. LWT 80:19–26. https://doi.org/10.1016/j.lwt.2017.01.072
55. Zapata RB, Villa AL, Correa CMD, Williams CT (2009) In situ Fourier transform infrared spectroscopic studies of limonene epoxidation over PW-Amberlite. Appl Catal Gen 365:42–47. https://doi.org/10.1016/j.apcata.2009.05.047
56. Jin F, Xie L, Zhang H, Fan X, Tian J, Liu W et al (2025) Dendritic Cells: Origin, Classification, Development, Biological Functions, and Therapeutic Potential. MedComm 6:e70455. https://doi.org/10.1002/mco2.70455
57. Lee M, Du H, Winer DA, Clemente-Casares X, Tsai S (2022) Mechanosensing in macrophages and dendritic cells in steady-state and disease. Front Cell Dev Biol 10:1044729. https://doi.org/10.3389/fcell.2022.1044729
58. Bürgel PHM, de Castro RJA, Basso AM, Coelho LC, Marina CLF, Siqueira IM et al (2025) Exopolysaccharides of Ganoderma lucidum Activate the NLRP3 Inflammasome, Modulating Phagocytes and the Response of Mice to Infection with Cryptococcus neoformans. Mycopathologia 190:49. https://doi.org/10.1007/s11046-025-00950-w
59. Carbonero ER, Novikov TSM, Gomes YGS, Brito DR, Coelho LC, Mendes MF et al (2024) Chemical Characterization and In Vitro Evaluation of Glucans from Fermentation-Produced Nutraceutical Bionutri-AR1®: Antioxidant and Immunomodulatory Properties. Pharmaceutics 16:1404. https://doi.org/10.3390/pharmaceutics16111404
60. Sakabe R, Onishi K, Mochizuki J, Toshimitsu T, Shimazu T, Kishino S et al (2025) Regulation of IL-10 production in dendritic cells is controlled by the co-activation of TLR2 and Mincle by *Lactiplantibacillus plantarum* OLL2712. Obar JJ, editor. Microbiol Spectr. ;13:e01196-24. https://doi.org/10.1128/spectrum.01196-24
61. Chu TW, Ho C-C, Chiu H-P, Hsu Y-J, Hung C-T, Sung C-H et al (2025) d-Limonene inhibits cytokines and chemokines expression by regulating NF-kappaB and STAT in HaCat cells and DNCB-induced atopic dermatitis in BALB/c mice. Int Immunopharmacol 148:114082. https://doi.org/10.1016/j.intimp.2025.114082
62. Rakoczy K, Szymańska N, Stecko J, Kisiel M, Maruszak M, Niedziela M et al (2025) Applications of Limonene in Neoplasms and Non-Neoplastic Diseases. Int J Mol Sci 26:6359. https://doi.org/10.3390/ijms26136359
63. Lau AW, Pineda JP, DeLouise LA (2023) Immunomodulatory Effects of Nanoparticles on Dendritic Cells in a Model of Allergic Contact Dermatitis - Importance of PD-L2 Expression [Internet]. In Review; [cited 2025 Dec 2]. https://doi.org/10.21203/rs.3.rs-3069059/v1
64. Sousa F, Lee H, Almeida M, Bazzoni A, Rothen-Rutishauser B, Petri-Fink A (2024) Immunostimulatory nanoparticles delivering cytokines as a novel cancer nanoadjuvant to empower glioblastoma immunotherapy. Drug Deliv Transl Res 14:2655–2667. https://doi.org/10.1007/s13346-023-01509-2
65. Coelho LC, Favilla LD, de Castro TB, Leal MCBDM, Hoffmann C, Bocca AL (2025) Auricularia auricula's Exopolysaccharide Mitigates DSS-Induced Colitis Through Dectin–1-Mediated Immunomodulation and Microbiota Remodeling. Pharmaceuticals 18:1085. https://doi.org/10.3390/ph18081085
66. Kathem SH, Nasrawi YSh, Mutlag SH, Nauli SM (2024) Limonene Exerts Anti-Inflammatory Effect on LPS-Induced Jejunal Injury in Mice by Inhibiting NF-κB/AP-1 Pathway. Biomolecules 14:334. https://doi.org/10.3390/biom14030334
67. Yu L, Yan J, Sun Z (2017) D-limonene exhibits anti-inflammatory and antioxidant properties in an ulcerative colitis rat model via regulation of iNOS, COX-2, PGE2 and ERK signaling pathways. Mol Med Rep 15:2339–2346. https://doi.org/10.3892/mmr.2017.6241
68. Jiang Y, Liu G, Liu Q, Zhang L, Tan Y, Cen J et al (2025) Related Mechanism of Limonene Improves LPS-Induced Neuroinflammation. J Microbiol Biotechnol 35:e2411053. https://doi.org/10.4014/jmb.2411.11053
69. Priyoatmojo D, Dewi RT, Septama AW, Angelina M, Yuliani T, Wahyono T (2025) Edible layer-by-layer electrostatic adsorption nano and microcapsules based on plant proteins as natural bioactive delivery systems: A review. Food Chem Adv 6:100861. https://doi.org/10.1016/j.focha.2024.100861
70. Badawy MEI, Lotfy TMR, Shawir SMS (2020) Facile synthesis and characterizations of antibacterial and antioxidant of chitosan monoterpene nanoparticles and their applications in preserving minced meat. Int J Biol Macromol 156:127–136. https://doi.org/10.1016/j.ijbiomac.2020.04.044
71. Alipanah H Chitosan nanoparticles containing limonene and limonene-rich essential oils: potential phytotherapy agents for the treatment of melanoma and breast cancers

Authors and Affiliations

Guilherme L. Alves[1] · Gislane O. Ribeiro[1] · Maria Carolina B. Di Medeiros[2] · Luciano M. Lião[2] · Luísa C. Coelho[3] · Anamélia L. Bocca[3,4,5] · Maria I.G. Leles[6] · Ricardo N. Marreto[7] · Kátia F. Fernandes[1]

✉ Kátia F. Fernandes
kfernandes.lqp@gmail.com

Guilherme L. Alves
guilhermea47@gmail.com

Maria Carolina B. Di Medeiros
caroldimedeiros@gmail.com

Luísa C. Coelho
luisa98@gmail.com

Anamélia L. Bocca
anamelia.bocca@gmail.com

Ricardo N. Marreto
rnmarreto@gmail.com

[1] Laboratório de Química de Polímeros, Departamento de Bioquímica e Biologia Molecular, Instituto de Ciências Biológicas, Universidade Federal de Goiás, Goiânia 74690-900, GO, Brazil

[2] Laboratório de Ressonância Nuclear Magnética, Instituto de Química, Universidade Federal de Goiás, Goiânia 74690-900, GO, Brazil

[3] Laboratório de Imunologia Aplicada, Departamento de Biologia Celular, Instituto de Ciências Biológicas, Universidade Federal de Brasília, Brasília 70910- 000, DF, Brazil

[4] Bi-Institutional Translational Medicine Platform, Oswaldo Cruz Foundation (Fiocruz), Ribeirão Preto 14049900, Brazil

[5] National Institute of Science and Technology in Human Pathogenic Fungi, Ribeirão Preto, São Paulo 14049900, Brazil

[6] Laboratório de Métodos de Extração e Separação LAMES, Instituto de Química, Universidade Federal de Goiás, Goiânia 74.690-900, GO, Brazil

[7] Laboratory of Nanosystems and Drug Delivery Devices (NanoSYS), School of Pharmacy, Federal University of Goias, Goiania 74605-170, GO, Brazil